The Company of Biologists

RESEARCH ARTICLE

Septate junction components control *Drosophila* hematopoiesis through the Hippo pathway

Rohan J. Khadilkar and Guy Tanentzapf*

ABSTRACT

Hematopoiesis requires coordinated cell signals to control the proliferation and differentiation of progenitor cells. In *Drosophila*, blood progenitors, called prohemocytes, which are located in a hematopoietic organ called the lymph gland, are regulated by the Salvador-Warts-Hippo pathway. In epithelial cells, the Hippo pathway integrates diverse biological inputs, such as cell polarity and cell-cell contacts, but *Drosophila* blood cells lack the conspicuous polarity of epithelial cells. Here, we show that the septate-junction components Cora and NrxIV promote Hippo signaling in the lymph gland. Depletion of septate-junction components in hemocytes produces similar phenotypes to those observed in Hippo pathway mutants, including increased differentiation of immune cells. Our analysis places septate-junction components as upstream regulators of the Hippo pathway where they recruit Merlin to the membrane. Finally, we show that interactions of septate-junction components with the Hippo pathway are a key functional component of the cellular immune response following infection.

KEY WORDS: Cell polarity, *Drosophila*, Hematopoiesis, Hippo signaling, Septate junctions

INTRODUCTION

The Hippo pathway is an evolutionarily conserved signaling pathway that regulates organ size by controlling cell proliferation, cell death and cell differentiation (Pan, 2010; Yu and Guan, 2013; Meng et al., 2016; Karaman and Halder, 2017). In flies, the core of the Hippo pathway is a phosphorylation cascade wherein a complex of Salvador (Sav) and Hippo (Hpo) phosphorylates and activates a complex of the kinase Warts (Wts) and its binding partner Mats. The key target of this phosphorylation cascade is the protein Yorkie, which is directly phosphorylated by activated Wts (Huang et al., 2005; Pan, 2010; Meng et al., 2016). Yorkie (Yki) can translocate to the nucleus where it acts as a co-activator, but its phosphorylation by Wts maintains it in the cytoplasm where it cannot regulate transcription. Multiple cellular cues feed into the core Hippo pathway, including planar and apicobasal cell polarity, mechanical force and cell-cell contacts (Pan, 2010; Yu and Guan, 2013; Meng et al., 2016; Elbediwy et al., 2016; Karaman and Halder, 2017). In particular, there are extensive mechanistic connections between the machinery that controls apical polarization in epithelial cells and the Hippo pathway (Pan, 2010; Meng et al., 2016; Karaman and Halder, 2017). Specifically, in epithelial cells, three apically

Department of Cellular and Physiological Sciences, University of British Columbia, Vancouver V6T 1Z3, Canada.

*Author for correspondence (tanentz@mail.ubc.ca)

R.J.K., 0000-0002-7297-2736; G.T., 0000-0002-2443-233X

polarized cytoplasmic proteins, Merlin (Mer), Expanded (Ex) and Kibra (Kib), are known to act upstream of the core Hippo pathway kinase cascade. Although initially shown to be able to bind each other (McCartney et al., 2000), Mer and Ex have since been shown to localize to the apical domain independently of each other, to be partially redundant and to form two spatially distinct apical complexes: Mer binds Kib, while Ex binds to the transmembrane apical protein Crumbs (Pan, 2010; Ling et al., 2010; Yu and Guan, 2013; Meng et al., 2016; Su et al., 2017). Crumbs has long been established to be an important regulator of apical polarization in epithelia (Tepass, 2012). In another example, planar cell polarity cues are linked to the Hippo pathway via the Fat/Dachsous (Ft/Ds) system. Ft and Ds are two protocadherins that play key instructive roles in the formation of planar cell polarity (Adler, 2002; Goodrich and Strutt, 2011; Sharma and McNeill, 2013; Matis and Axelrod, 2013). Ft has been proposed to regulate Hippo signaling by controlling the membrane localization and/or stability of Ex (Bennett and Harvey, 2006; Silva et al., 2006; Willecke et al., 2006). More recently, Ft and Ex were shown to function in parallel to regulate Wts stability and activity (Cho et al., 2006; Feng and Irvine, 2007).

In epithelial cells in vertebrates there is a well-established connection between the occluding, permeability barrier forming cell-junctions, tight junctions (TJs) and Hippo signaling (Karaman and Halder, 2017). For example, one link between TJs and Hippo signaling occurs through a protein complex composed of Mer, the scaffolding protein Angiomotin (Amot), and the Crumbs-binding proteins Patj and Pals1 (Yi et al., 2011; Karaman and Halder, 2017). Amot binds to the vertebrate Yorkie orthologs Yap and Taz, and functions to keep them out of the nucleus (Chan et al., 2011; Zhao et al., 2011; Karaman and Halder, 2017). Amot protein also binds to and recruits the vertebrate Wts orthologs Lats1 and Lats2 to the cell membrane, which facilitates their activation. Another link between the Hippo pathway and TJs occurs through the TJ-associated protein ZO-2, which binds to both Yap and Taz, and modulates their ability to enter the nucleus (Oka et al., 2010; Karaman and Halder, 2017). In *Drosophila*, the links between the Hippo pathway and septate junctions (SJs), the functional homologues to TJs, are not very well established. To date, neither of the two core components of fly SJs, Coracle and NrxIV, has been implicated in Hippo signaling, although the SJ-associated protein Dlg (Woods and Bryant, 1991), together with its complex partners Lgl and Scrib, act as upstream regulators of the Hippo pathway (Grzeschik et al., 2010; Grusche et al., 2011; Sun and Irvine, 2011; Chen et al., 2012; Verghese et al., 2012; Karaman and Halder, 2017). Nonetheless, the precise role of SJs in Hippo signaling in flies has not been defined.

The Hippo pathway is known to regulate hematopoiesis in flies (Milton et al., 2014; Ferguson and Martinez-Agosto, 2014a,b). Flies have two branches of the immune system: the humoral arm, which is based on the production of antimicrobial peptides, notably from the fat body (Hoffmann et al., 1993); and the cellular arm, which is

based on the production of phagocytic immune cells called hemocytes that attack, engulf and neutralize pathogens and other immune challenges (Defaye et al., 2009). In *Drosophila* larva, the main site where immune cells are produced is the primary lobe of the lymph gland (LG). The primary lobe contains three distinct zones: the posterior signaling center (PSC) houses the hematopoietic niche; the medullary zone (MZ) houses progenitor cells known as prohemocytes; and the cortical zone (CZ) that contains the differentiated blood cells (Jung et al., 2005). There are three types of hemocytes found in flies: plasmatocytes are phagocytic cells that engulf pathogens; crystal cells are involved in the melanization response; and lamellocytes are specialized cells that fight parasites (Evans et al., 2003; Jung et al., 2005). The PSC provides a specialized micro-environment producing signals that regulate prohemocyte differentiation (Krzemień et al., 2007). A number of signaling pathways act in the LG to regulate hematopoiesis, including Wingless, Hedgehog, JAK/STAT, BMP and Notch (Lebestky et al., 2003; Krzemień et al., 2007; Mandal et al., 2007; Sinenko et al., 2009; Kulkarni et al., 2011; Pennetier et al., 2012; Sinha et al., 2013; Khadilkar et al., 2014; Khadilkar et al., 2017a,b). Mutations that perturb these signaling pathways can result in either an inability to produce hemocytes or in ectopic overproduction of hemocytes.

The Hippo pathway regulates hematopoiesis in the LG by controlling the differentiation and proliferation of hemocytes (Milton et al., 2014; Ferguson and Martinez-Agosto, 2014a,b). Loss of Wts results in ectopic, premature, and abnormal differentiation of prohemocytes into crystal cells and plasmatocytes in the LG. These defects were shown to occur because of two potentially related mechanisms. First, downstream of Wts, changes in the expression of Lozenge, an important regulator of crystal cell fate, are mediated by the transcriptional activity of Yorkie (Milton et al., 2014; Ferguson and Martinez-Agosto, 2014b). Second, hyper-activation of Yorkie results in ectopic crystal cell production by modulating the Notch pathway (Ferguson and Martinez-Agosto, 2014b). Hippo pathway signaling and, in particular, Yorkie were also shown to be essential for regulating circulating hemocyte proliferation in a melanotic tumor model induced by ectopic activation of JAK/STAT signaling (Anderson et al., 2017). Finally, the Yorkie binding partner Scalloped was shown to regulate prohemocyte maintenance and proliferation through PVR signaling (Ferguson and Martinez-Agosto, 2017). In addition to regulating immune cell production, the Hippo pathway is an important regulator of the humoral immune response. In particular, Yorkie directly regulates the transcription of antimicrobial response genes in the fly (Liu et al., 2016). Moreover, Gram-positive bacteria act as extracellular stimuli that initiate the production of antimicrobial peptides by modulating Hippo signaling subsequent to infection (Liu et al., 2016).

Previous work from our lab has demonstrated that the core SJ components NrxIV and Cora are expressed in the lymph gland where they form occluding junctions that act as a permeability barrier around the PSC. This permeability barrier plays an important role in the lymph gland by regulating the accessibility of prohemocytes to PSC-derived signals (Khadilkar et al., 2017b). The immune response triggered by infection causes the permeability barrier to break down, altering the prohemocyte microenvironment to induce hemocyte production. Moreover, genetically induced barrier ablation provides protection against infection by activating the immune response (Khadilkar et al., 2017b). In this present work, we have extended on these earlier findings and show that NrxIV and Cora also play an important role in regulating Hippo signaling in differentiating and mature hemocytes to control their behavior. Specifically, we find that Cora and NrxIV act as upstream regulators of Hippo signaling in the crystal cell lineage. Similar phenotypes, including increased differentiation of crystal cells, are seen upon loss of *cora* and *NrxIV*, or in response to the specific inactivation of the Hippo pathway in hemocytes. We observed extensive genetic interactions between Cora/NrxIV and Hippo pathway components. Analysis of these interactions revealed that Cora and NrxIV act downstream or in parallel to Ft but upstream of Mer and Ex. Finally, we show that Cora and the Hippo pathway have an important function in the hemocytes in initiating the cellular immune response following infection. In particular, induction of the cellular immune response requires the inactivation of the Hippo pathway, which occurs via downregulation of Cora in the hemocytes. Our results show that SJ components modulate Hippo signaling in the LG and this mechanism controls the induction of the cellular immune response following infection.

RESULTS
Similar phenotypes are produced by depletion of either Hippo pathway genes or SJ components in the LG
While dissecting LGs from larva heterozygous for alleles of *cora* and *NrxIV*, we noticed that they were enlarged. Intriguingly, changes in LG size have previously been associated with changes in levels of Hippo pathway genes (Milton et al., 2014). To investigate this further, the overall size of the LG was measured by counting the total number of cells in the organ in larva heterozygous for mutations in the SJ component *cora*, in homozygous mutants of the Hippo pathway component*s fat* and *wts*, or in heterozygous *yorkie* mutants (Fig. 1A,A′,B′,D′,F,G). This analysis confirmed that similar LG enlargement occurred in Hippo pathway mutants or upon Cora depletion; in comparison, and consistent with previous reports (Milton et al., 2014), the size of the LGs in heterozygous *yorkie* mutants was slightly lower than wild type (Fig. 1F,G). A similar phenotype of increased overall LG size was observed for heterozygous Hippo pathway mutants (Fig. 1B,D,G). Developmental analysis of LG organ size in *cora* and *NrxIV* mutants showed the enlarged LG phenotype was already present in first instar larva and was not simply the result of post-embryonic growth of the LG (Fig. S1A-C″). This suggested that the enlarged LGs in *cora* mutants represented a true defect in organ size, characteristic of Hippo pathway mutants. Previous work on the *wts* gene showed that Hippo signaling is important in regulating the differentiation of prohemocytes into crystal cell lineage (Milton et al., 2014). Consistent with this, larva homozygous mutant for the Hippo pathway genes *fat* and *wts* exhibited a significant increase in the number of differentiated crystal cells, as indicated by Hnt staining, even when taking into account their overall larger size (Fig. 1J,L,N). Surprisingly, a robust crystal cell differentiation phenotype was observed even in larva heterozygous mutant for the Hippo pathway genes *fat* and *wts*, indicating that the LG is very responsive to the level of Hippo signaling, although these phenotypes were somewhat weaker than those observed in homozygous mutants (Fig. 1I′,K′,N). Two lines of evidence suggest that these defects were unlikely due to the genetic background effects. First, both the lymph gland size and crystal cell differentiation phenotypes observed in homozygous *wts* mutants were rescued by ectopic expression of *wts* via a prohemocyte driver (Fig. 1D′-E′,G,L-M,N). Second, transheterozyote combinations of different *wts* alleles exhibited similar defects in LG size and crystal cell differentiation (Fig. 1C,C′,G,J′,K,N). In comparison with the phenotypes seen in *fat* and *wts* mutants, larva heterozygous for alleles of *yorkie* showed a slightly lower number of differentiated
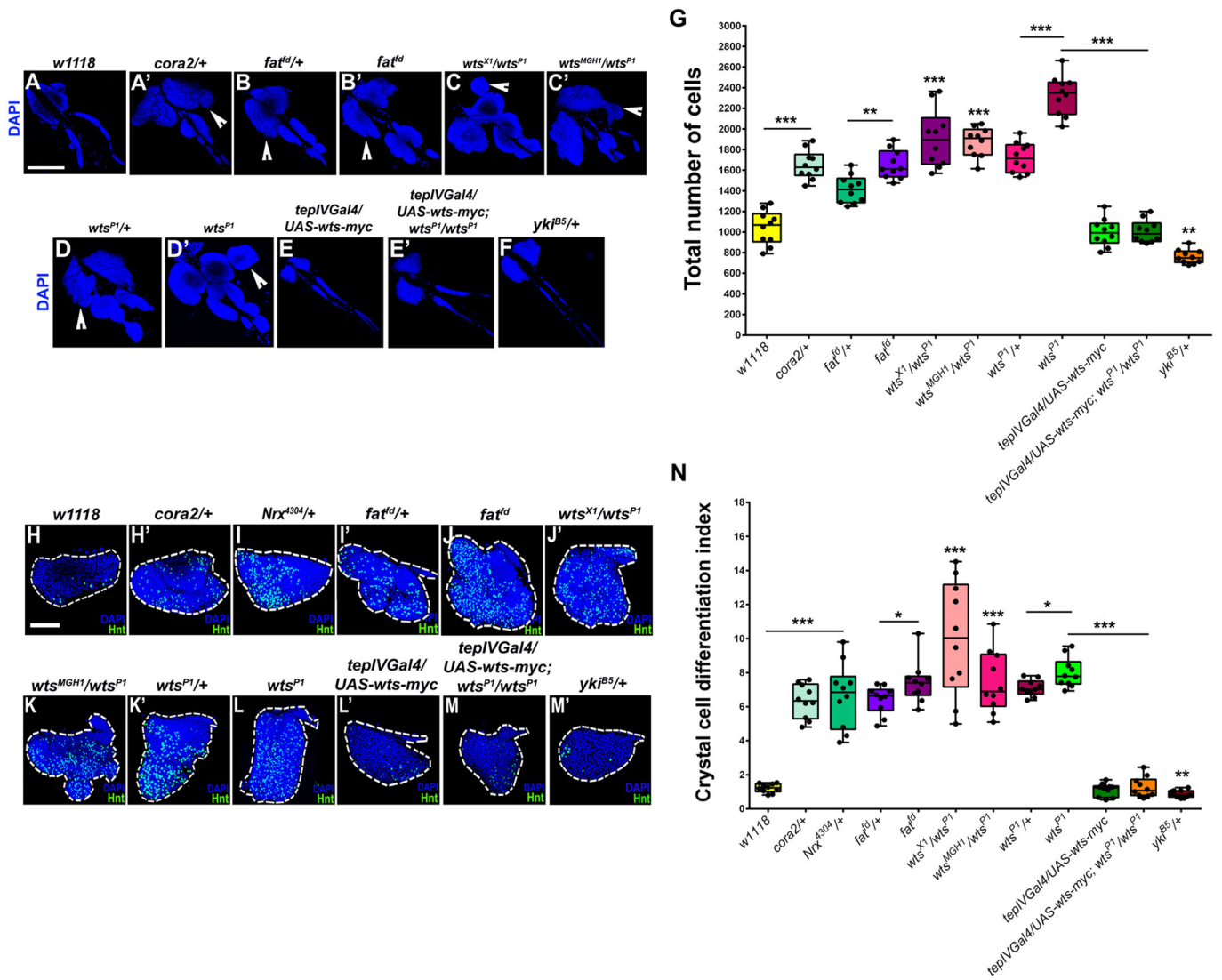
Fig. 1. Similar phenotypes are produced by depletion of either Hippo pathway genes or SJ components in the LG. (A-F) Representative whole lymph glands in wild-type control larvae (*w1118*; A) and in larvae heterozygous or homozygous for mutant alleles of *coracle* (*cora2/+*; A′), *fat* (*fat^fd^/+* or *fat^fd^*; B,B′) and *warts* (*wts^P1^/+* or *wts^P1^*; D,D′); transheterozygous combinations of *warts* alleles (*wts^X1^/wts^P1^* or *wts^MGH1^/wts^P1^*; C,C′); upon over-expression of Warts in prohemocytes alone or in *warts* mutant genetic background (*tepIVGal4/UAS-wts-myc* or *tepIVGal4/UAS-wts-myc; wts^P1^/wts^P1^*; E,E′); and in *yorkie* (*yki^B5^/+*; F). (G) Quantification of total number of cells in the LG for genotypes shown in A-F (see supplementary Materials and Methods). (H-M) Representative primary lymph gland lobes labeled for the crystal cell marker Hindsight (Hnt; green) from wild-type control larvae (*w1118*; H) and in larvae heterozygous or homozygous for mutant alleles of *coracle* (*cora2/+*; H′), *NrxIV* (*Nrx^4304^/+*; I), *fat* (*fat^fd^/+ or fat^fd^*; I′,J) and *warts* (*wts^P1^/+* or *wts^P1^*; K′,L); in transheterozygous combinations of *warts* alleles (*wts^X1^/wts^P1^* or *wts^MGH1^/wts^P1^*; J′,K); upon overexpression of Warts in prohemocytes alone or in *warts* mutant genetic background (*tepIVGal4/UAS-wts-myc* or *tepIVGal4/UAS-wts-myc; wts^P1^/wts^P1^*; L′,M); and in *yorkie* (*yki^B5^/+*; M′). (N) Quantification of the crystal cell differentiation index (in arbitrary units) for genotypes shown in H-M′. Boxes in the box and whisker plots in G and N span the interquartile range. Horizontal lines indicate median for the total number of cells and crystal cell differentiation index. Individual points on the plot indicate individual data points and the whiskers go from each quartile to the minimum or maximum. Plots show data for total number of cells (G) and crystal cell differentiation indices (N). Statistical significance was estimated using unpaired *t*-test with Welch's correction. White arrowheads indicate the lymph gland tissue overgrowth in the mutants when compared with the control. Error bars indicate s.d. of the mean. All the mutants, including the transheterozygotes, were compared with the wild-type control. Homozygous mutant data were compared with the heterozygotes and the wild-type controls. Rescue data involving overexpression of Warts in the *warts* mutant background was compared with the *warts* mutant data and the overexpression sample alone. ***$P<0.001$, **$P<0.01$ and *$P<0.1$. Nuclei in A-F and H-M′ are stained with DAPI (blue). Scale bars: 100 μm in A-F; 40 μm in H-M′. See also Fig. S1.

crystal cells when compared with wild type (Fig. 1H,M′,N). Importantly, an increase in the number of differentiated crystal cells was also observed in larva heterozygous for alleles of *cora* or *NrxIV* (Fig. 1H,H′,I,N). An additional phenotype previously described for *wts* mutants was the presence of hemocytes that expressed markers for more than one of the *Drosophila* blood cell lineages (Milton et al., 2014). Specifically, hemocytes were found that expressed both plasmatocyte and crystal cell markers, such as P1 and Lozenge,

respectively. Such mixed lineage hemocytes were not observed in controls but were present when either of the Hippo pathway components Cora and NrxIV was depleted in the LG using either of the following two different approaches: RNAi-mediated knockdown or the introduction of one copy of a mutation in *fat*, *wts* or *cora* (Fig. S3A-L). Taken together, these results show a striking similarity in the phenotypes observed in the LG upon depletion of *cora* or *NrxIV*, or when the Hippo pathway was inactivated.

Cora functions in blood progenitors to regulate LG size

Previously, we have shown that Cora and NrxIV function in the PSC. To determine whether the organ size defects in *cora* mutants were due to its action in the PSC, a series of rescue experiments were carried out. Because null *cora* mutants are embryonic lethal, these experiments were carried out in heterozygous *cora* mutants, as these exhibit robust phenotypes (Fig. 1A′,G,H′,N). In these experiments, specific drivers for the PSC (*collier*-GAL4; Krzemien et al., 2007), prohemocytes (*tep4*-GAL4; Jung et al., 2005; Avet-Rochex et al., 2010) and differentiated crystal cells (*lz*-GAL4; Lebestky et al., 2000) were used to drive UAS-Cora in larva heterozygous for an allele of *cora* (see supplementary Materials and Methods, Fig. S13-S15). These experiments showed that restoring full Cora levels to the PSC, prohemocytes or differentiated crystal cells rescued different aspects of the *cora* mutant phenotype. Specifically, restoring Cora function specifically in the PSC rescued the previously described increased PSC cell number (Khadilkar et al., 2017b) but not overall LG size (Fig. S13A-E,K-O). In contrast, restoring Cora levels specifically in the prohemocytes did not rescue PSC cell numbers but rescued LG size (Fig. S14A-E,K-O). Finally, restoring Cora levels specifically in the differentiated crystal cells did not rescue either PSC cell numbers or LG size (Fig. S15A-E,K-O). Intriguingly, crystal cell differentiation defects were rescued by restoring Cora levels in either the PSC, prohemocytes or differentiated crystal cells (Figs S13-15F-J). This could be because in the heterozygous *cora* mutant background, Cora is still present in the LG which makes rescuing some, more-sensitive, aspects of the phenotype easier. Overall, this analysis suggests a distinct function of *cora* outside the PSC.

The Hippo pathway, Cora and NrxIV function in the crystal cell lineage to regulate differentiation

As the Hippo pathway mutant *wts* has previously been reported to be important for crystal cell differentiation (Milton et al., 2014), we wanted to further test whether Cora and NrxIV activity was required in that particular lineage. A specific driver for the crystal cell lineage, *lozenge*-GAL4 (*lz*-GAL4), was used to drive RNAi transgenes targeting the Hippo pathway genes *fat*, *hpo*, *wts*, *mer* and *ex*, as well as *cora* and *NrxIV*. Depleting either Hippo pathway components or Cora and NrxIV in the crystal cell lineage resulted in a substantial increase in the production of crystal cells (Fig. S2A-H). A subset of these results was confirmed using an alternative crystal cell driver, *pebbled*-GAL4 (Sweeney et al., 2007; Fig. S2I-M). The *lz*-GAL4 driver is broadly expressed in the crystal cell lineage and could therefore be inducing RNAi-mediated depletion of Hippo pathway components or Cora and NrxIV in either differentiating progenitor cells or in fully differentiated crystal cells (Lebestky et al., 2000). As previous reports suggested that the Hippo pathway was required in the progenitor population (Milton et al., 2014), it was decided to further refine when the Hippo pathway components, and Cora and NrxIV were acting. To achieve this, two additional drivers that are specifically expressed in either the prohemocyte stage (*tep4*-GAL4) or the differentiating hemocyte stage (*Pxn*-GAL4; Krzemień et al., 2010; Minakhina et al., 2011) were used to drive RNAi transgenes to deplete Cora and NrxIV. A large increase in the production of crystal cells (marked by Hnt) was observed when either *tep4*-GAL4 or *Pxn*-GAL4 was used to deplete Cora or NrxIV (Fig. 2A-H). To confirm that this effect was cell autonomous and not due to global changes in the tissue experiments, clonal analysis was carried out. Specifically, we induced *cora* mutant clones in the LG (see supplementary Materials and Methods). Of

102 *cora* mutant cells analyzed, 30 (~30%) were differentiated into Hnt-positive crystal cells. In contrast, in a comparable population of cells without the *cora* mutation few (four out of 155 or 2.6%) were Hnt-positive crystal cells (Fig. S12A-F).

Cora function also appeared to play an important role in allowing cells in the crystal cell lineage to establish or maintain their identity. RNAi-mediated knockdown of *cora* in the crystal cells using *lz*-Gal4 resulted in cells that showed mixed lineage fate as they expressed the plasmatocyte marker P1 (Fig. S3E-L). In comparison, knocking down *cora* or *wts* specifically in plasmatocytes using UAS-*cora*-RNAi or UAS-*wts*-RNAi line driven by *eater*-GAL4 does not produce mixed lineage cells (Tokusumi et al., 2009; see supplementary Materials and Methods; Fig. S3Q-S). Moreover, co-expressing *cora* RNAi in crystal cells along with an active form of the crystal fate determinant Klumpfuss, which is known to suppress plasmatocyte characteristics (Terriente-Felix et al., 2013), suppressed these differentiation defects (Fig. S3M-P′). These results show that the Hippo pathway, Cora and NrxIV control crystal cell differentiation in the LG and that their function may be required in hematopoietic progenitors.

Yorkie is transcriptionally active in the LGs of *cora* mutants

The phenotypic similarity between Hippo pathway, Cora, and NrxIV mutants is consistent with a functional interaction between the Hippo pathway and SJ components. To explore this further, two different transgenic reporters, one for the gene *four jointed* (*fj-lacZ*; Villano and Katz, 1995; Brodsky and Steller, 1996; Zeidler et al., 1999; Zeidler et al., 2000) and the other for the microRNA *bantam* (*bantam*-GFP; Brennecke et al., 2003), were used to assay the activity of Hippo pathway in larva heterozygous for an allele of *cora*. The *fj-lacZ* reporter is expressed in response to Yorkie activity (Cho et al., 2006; Matakatsu et al., 2017). Since Yorkie activity is reported to promote crystal cell fate (Milton et al., 2014; Ferguson and Martinez-Agosto, 2014a,b) we confirmed that, compared to a LacZ control, *fj*-LacZ-positive cells expressed the crystal cell marker Hnt but not a label for prohemocytes (*tep4*-GAL4 driving UAS-GFP; Fig. S10A-L). Larva heterozygous for alleles of either of the Hippo pathway genes *fat*, or *wts* or *cora* exhibited a significant increase in the number of cells expressing high levels of *fj-lacZ* in the LG compared to wild-type controls or *yorkie* mutants (Fig. 3A-E and K). The expression of another reporter for Hippo activity, *bantam*-GFP, is reduced in Hippo pathway mutants (Thompson and Cohen, 2006; Nolo et al., 2006). It has been reported that *bantam*-GFP levels are lowered by the presence of the *bantam* microRNA, and we confirmed this using a LacZ reporter for *bantam* microRNA expression that this is also the case in the LG (Huang et al., 2013; Huang et al., 2014; Fig. S6E-F″). We also show that the bantam-LacZ cells are positive for the crystal cell marker Hnt (Fig. S6G-G″). Moreover, expressing a microRNA sponge targeting the *bantam* microRNA leads to increased levels of *bantam*-GFP (Becam et al., 2011; Fig. S6C-D″). Finally, *bantam*-GFP is active in prohemocytes but is inactive in differentiated crystal cells (Fig. S6A-B″). Larva heterozygous for alleles of either of *fat* or *cora* exhibited a significant decrease in the number of cells expressing high levels of *bantam*-GFP in the LG compared with wild-type controls or *yorkie* mutants (Fig. S6H-K). One caveat in these experiments is that the *bantam*-GFP and *fj-lacZ* reporters could act in this context as markers for the crystal cell fate rather than Yki activity. Nonetheless, these data argue that the Hippo signaling cascade is inactivated in the LGs of *cora* mutants leading to Yki activation. Consistent with this idea, and based on the finding of Milton et al. (Milton et al., 2014) showing that Yki levels

tep4-Gal4 mediated SJ depletion
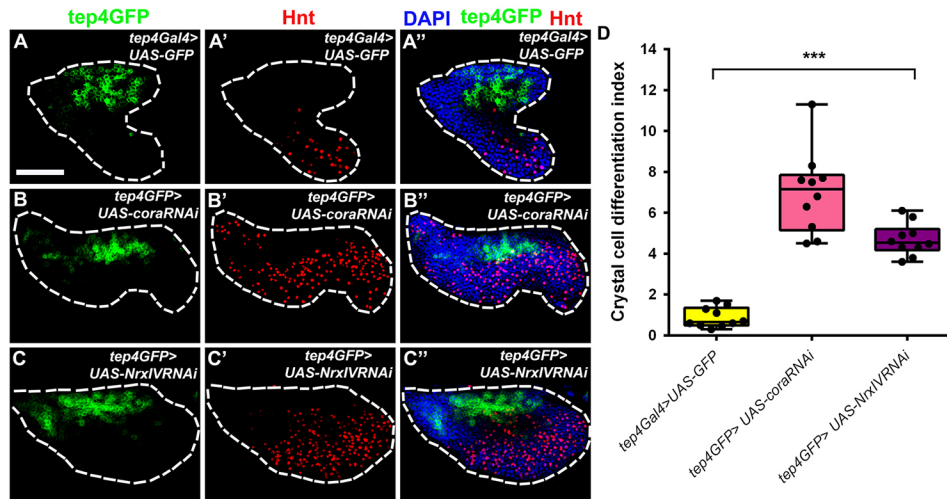
Pxn-Gal4 mediated SJ depletion
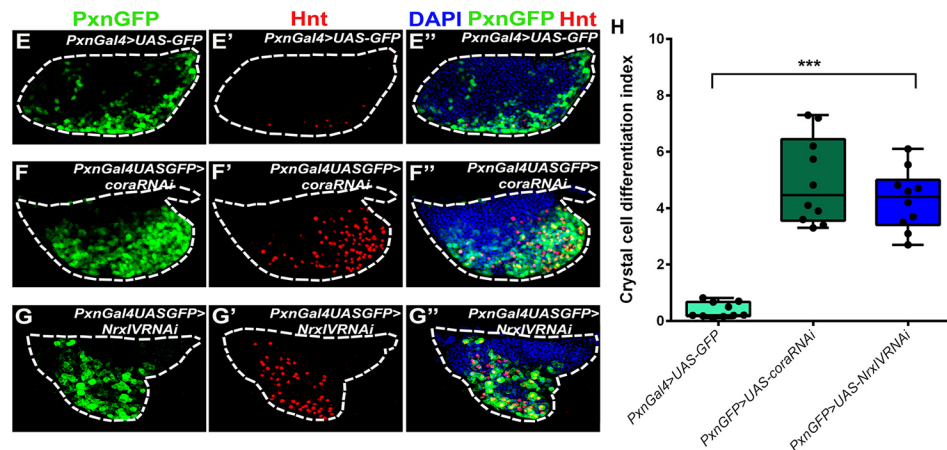
Fig. 2. Cora and NrxIV regulate the differentiation of crystal cells. (A-D) Crystal cell differentiation in representative control (UAS-GFP; A-A″) primary lymph glands and following knockdown of *cora* (B-B″) and *NrxIV* (C-C″) driven by the prohemocyte-specific driver *tep4-Gal4*. Crystal cells are labeled for Hnt (red); prohemocytes are labeled by the expression of UAS-GFP (green). (D) Quantification of the crystal cell differentiation index (in arbitrary units, see supplementary Materials and Methods) for genotypes shown in A-C″. (E-G″) Crystal cell differentiation in representative control (UAS-GFP; E-E″) primary lymph glands and following knockdown of *cora* (F-F″) and *NrxIV* (G-G″) driven by the intermediate differentiating hemocyte-specific driver *Pxn-Gal4*. Crystal cells labeled for Hnt (red), prohemocyte labeled by expression of UAS-GFP (green). (H) Quantification of the crystal cell differentiation index (in arbitrary units) for genotypes shown in E-G″. Nuclei are marked with DAPI (blue). Statistical significance was estimated using an unpaired *t*-test with Welch's correction. Error bars indicate s.d. of the mean. The boxes in the box and whisker plot denote the interquartile range of the data. Horizontal lines represent the median and the points show the individual data points. Whiskers are the lines outside the box that extend to the highest and lowest data values. Plot shows data for the crystal cell differentiation indices. ***$P<0.001$. Scale bars: 40 μm in A-C″,E-G″. See also Figs S2 and S3.

correlate with Hippo pathway activity in the LG, Yorkie expression was analyzed and found to be higher in *coracle* mutant cell clones in the LG (see supplementary Materials and Methods; Fig. S12G-L). It should be noted, however, that in both our experiments and those of Milton and colleagues, Yorkie appeared to be mostly cytoplasmic in the LG cells, raising the possibility that Yki can act in a Hippo-independent parallel pathway.

Genetic interactions between SJ components and Hippo pathway components in crystal cell differentiation

Next, the functional relationship, as it pertains to crystal cell production, between Cora, NrxIV and the Hippo pathway was explored using genetic interaction studies. Removing one copy of the Hippo pathway genes *fat* and *wts* from larva heterozygous for an allele of *cora* enhanced their LG phenotype as the crystal cell differentiation index was elevated by ~20% (Fig. S4A-E). In contrast, removing one copy of *yorkie* robustly suppressed the crystal cell differentiation phenotypes of larva heterozygous for alleles of *cora* and *NrxIV* to the same degree that it suppressed similar phenotypes in larva heterozygous for alleles of *fat* (Fig. 3F-J,L). Importantly, similar phenotypic rescue could be obtained by using RNAi, which is expressed exclusively in the crystal cell lineage with the *lz-GAL4* driver, to knock down the *yorkie* gene in combination with either *cora*, *NrxIV*, *fat*, *hpo* or

wts (Fig. 3M, Fig. S5A-G′). Together, these data show robust genetic interaction in the crystal cell lineage between the Hippo pathway components and Cora or NrxIV. Moreover, these data suggest that a disruption in the Hippo pathway is a key causative agent for loss-of-function phenotypes of *cora* and *NrxIV* in LG hemocytes.

### Cora acts upstream of Ex and Mer

To identify the precise step in the Hippo pathway that was dependent on Cora and NrxIV, additional genetic interaction studies were carried out. First, we assayed whether ectopically activating the Hippo pathway at each step in the Hippo signaling cascade rescued the crystal cell phenotypes associated with RNAi-mediated *cora* knockdown. To activate the Hippo pathway, we used the crystal cell driver *lz*-GAL4 to overexpress the genes *fat*, *wts*, *mer* or *ex* in the crystal cell lineage. This analysis showed that activating Hippo downstream of *fat*, *ex*, *mer* or *wts* was able to restore crystal cell differentiation to wild-type levels following depletion of Cora (Fig. 4A-G). In contrast, ectopically overexpressing full-length Cora had no effect on the crystal cell differentiation phenotypes observed when Hippo signaling was inactivated at each step in the pathway (Fig. 4H). These data suggest that Cora activity occurs near the top of the Hippo signaling cascade and are consistent with Cora acting through or in parallel to Ex and/or Mer.
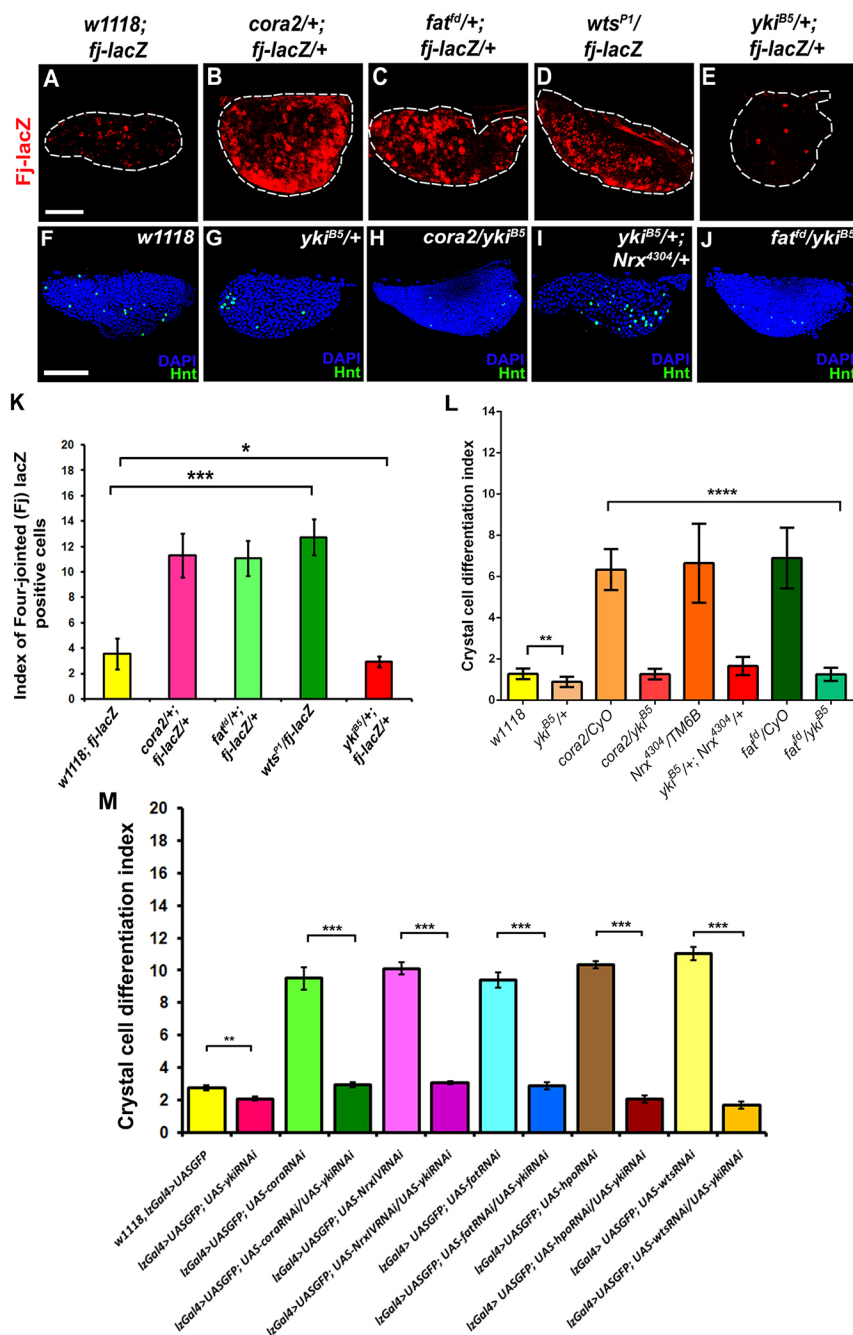
Fig. 3. Yorkie is transcriptionally active in the LGs of *cora* and *NrxIV* mutants. (A-E) Expression of the reporter transgene Four-jointed lacZ (*Fj-lacZ*, red; A-E) in representative larval primary lymph glands from wild-type control (*w1118*; A) or larvae heterozygous for mutant alleles of *cora* (*cora2/+*; B), *fat* (*fat^{fd}/+*; C), *warts* (*wts^{P1}/+*; D) or *yorkie* (*yki^{B5}/+*; E). (K) Quantification of Fj transcription represented as a Fj-lacZ-positive cells index (in arbitrary units, see supplementary Materials and Methods) for genotypes shown in A-E. (F-J) Representative primary lymph glands labeled for the crystal cell marker Hindsight (Hnt; green) from wild-type control larvae (*w1118*; F), larvae heterozygous for a mutant allele of *yorkie* (*yki^{B5}/+*; G), and in trans-heterozygous larvae mutant for alleles of *cora2/yki^{B5}* (H), *yki^{B5}/+; Nrx^{4304}/+* (I) and *fat^{fd}/yki^{B5}* (J). (L) Quantification of the crystal cell differentiation index (in arbitrary units) for the genotypes shown in F-J. (M) Quantification of crystal cell differentiation index following *lz-Gal4*-mediated crystal cell-specific knockdown of *yorkie* alone or in combination with the knockdown of *cora*, *NrxIV*, *fat*, *hippo* or *warts*. Nuclei are stained with DAPI (blue). Statistical significance was estimated using an unpaired *t*-test with Welch's correction. Data are mean± s.d. ****P<0.0001, ***P<0.001, **P<0.05 and *P<0.1. Scale bars: 40 μm in A-J. See also Figs S4, S5, S6, S10-S11.

To learn more about how Cora affects the Hippo pathway, we investigated whether the localization of Cora to the plasma membrane was required for the localization of Ft, Mer or Ex, and vice versa. Intriguingly, the cortical recruitment of Cora in the LG hemocytes was reduced in homozygous *fat* mutants. In contrast, Cora was normally localized to the cortex in the LG of homozygous mutants for *mer* or the downstream Hippo component *wts* (Fig. 5A-F). In a complementary set of experiments, the localization of Fat and GFP-tagged Mer or Ex was studied in the LG of larva heterozygous for an allele of *cora* (Fig. 5G-L and Fig. S7A,B,F). Mer-YFP colocalized with Cora at the cell membrane and cortical levels of Mer-YFP were severely diminished in hemocytes in the LG of larva heterozygous for an allele of *cora* (Fig. S11E-F″). The loss of cortical Mer was likely due to a change in its subcellular localization and not due to an overall reduction

or instability of the protein, as western blot analysis revealed similar overall Mer levels in larval LGs from either wild-type or heterozygous *cora* mutants with no evidence of protein degradation (Fig. 5J-M). Studying Ex-YFP localization proved more challenging, as Ex-YFP appeared as puncta in hemocytes in the LG (Fig. S11C-C″,G-G″). Co-labeling LG hemocytes with Pvr (PDGF-VEGF receptor), as a cortical marker, in addition to either Cora, Mer-YFP or Ex-YFP illustrated the strong cortical distribution of Cora and Mer and the largely cytoplasmic staining of Ex (Fig. S11A-H″). Nonetheless, we observed a general reduction in Ex levels in larval LGs from heterozygous *cora* mutants (Fig. 5G-I and Fig. S11C-D″,G-H″). The recruitment of Ft was also assayed in LGs in larva heterozygous for an allele of *cora* but these experiments were somewhat difficult to interpret due to cytoplasmic, punctate nature of Fat staining observed throughout

6
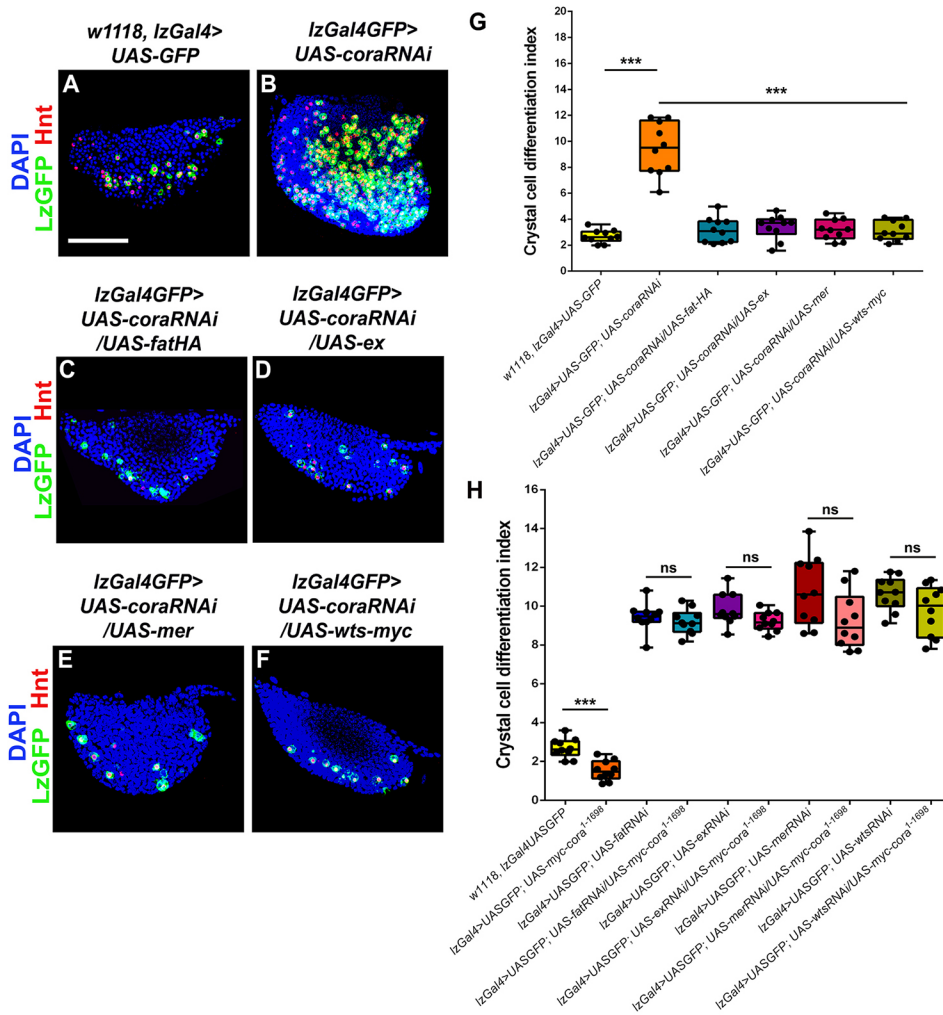
Fig. 4. Genetic interactions between Cora and Hippo pathway components. (A-F) Crystal cell differentiation in representative control primary lymph glands (UAS-GFP; A) and following crystal cell-specific (*lz-Gal4* driven) knockdown of *cora* alone (B) or combined with UAS lines to induce ectopic expression of *fat* (C), *ex* (D), *mer* (E) or *wts* (F). Crystal cells are labeled for Hnt (red), *lz-Gal4* expression is marked using UAS-GFP (green) and nuclei are stained using DAPI (blue). (G) Quantification of the crystal cell differentiation index (in arbitrary units) for genotypes shown in A-F. (H) Quantification of crystal cell differentiation index (in arbitrary units) in primary lymph glands following RNAi-mediated, crystal cell-specific (*lz-Gal4* driven) knockdown of *fat*, *ex*, *mer* and *wts* either alone or in combination with ectopic overexpression of Cora (using *UAS-myc-cora$^{1-1698}$*). Statistical significance was estimated using unpaired *t*-test with Welch's correction. Error bars indicate s.d. of the mean. ***P<0.001; ns, non-significant. The boxes in the box and whisker plot denote the interquartile range of the data. Horizontal lines represent the median and the points show the individual data points. Whiskers are the lines outside the box that extend to the highest and lowest data values. Plot shows data for the crystal cell differentiation indices. Scale bar: 40 µm in A-F.

the LG cells, as previously reported (Milton et al., 2014; Fig. S9A). Attempts to co-label Fat in prohemocytes using CD8-GFP driven by *tep4-Gal4* as a cortical marker were not informative, as CD8-GFP itself produces a heavy cytoplasmic staining in these cells (Fig. S9A). To confirm that the cytoplasmic punctate staining we obtained for Fat was real, we validated the antibody we used. This was carried out by confirming that this antibody was cortical in epithelial cells and detecting a signal that was increased or decreased by overexpressing or knocking down Fat in the LG prohemocytes, respectively (Fig. S9B-D). These results strongly argue for the specificity of this antibody, raising the possibility that the punctate staining observed in the LG corresponds to the recently described recruitment of the C-terminal domain of Fat to mitochondria (Sing et al., 2014). Nonetheless, there was no obvious difference in Ft staining between LGs from larva with reduced levels of Cora, larva with reduced levels of Wts or wild-type controls (Fig. S7A-F; Milton et al., 2014). Taken together, these results are consistent with Cora acting near the top of the Hippo pathway, upstream of Ex/Mer, although they do not completely rule out the possibility that Cora may also act in parallel to the Hippo pathway.

Hemocytes do not exhibit distinct apicobasal polarity
Expanded and Merlin, which, like Coracle, are members of the FERM (F for band 4.1-Ezrin-Radixin-Moesin) domain-containing

family of proteins, interact with regulators of epithelial cell polarity such as the Crumbs complex and are apically localized (Yu and Guan, 2013; Karaman and Halder, 2017). We therefore asked whether hemocytes in the LG exhibited the kind of conspicuous polarization that is characteristic of epithelial cells. We were unable to detect the apical polarity markers Crumbs or Bazooka in the cell cortex of LG hemocytes (Fig. 6A-D″) but the lateral domain markers Discs Large (Dlg) and Scribbled (Scrib) exhibited cortical distribution. Intriguingly, Scrib and Dlg were found throughout the cell cortex in LG hemocytes, colocalizing with Cora (Fig. 6E-H″). Similar data have been reported previously for DE-Cadherin in the LG (Jung et al., 2005). DE-Cadherin is a lateral marker in *Drosophila* epithelia that concentrates at the sub-apical region (Tepass, 2012). Intriguingly, components of the lateral polarity machinery are functionally required in the LG to control crystal cell differentiation (Fig. 6I-P). Specifically, reducing the levels of *scrib* or *dlg*, using either RNAi-mediated knockdown in prohemocytes or by introducing a heterozygous null mutation in these genes, caused increased crystal cell differentiation (Fig. 6I-P). Moreover, it was shown that, in the LG, DE-Cadherin plays a role in maintaining prohemocyte multipotency and preventing lamellocyte differentiation (Gao et al., 2013, 2014). These results suggest the machinery that regulates apical cell polarity in epithelial cells is absent in hemocytes in the LG but that lateral polarity proteins are found throughout the cell cortex and are functionally important.

DEVELOPMENT
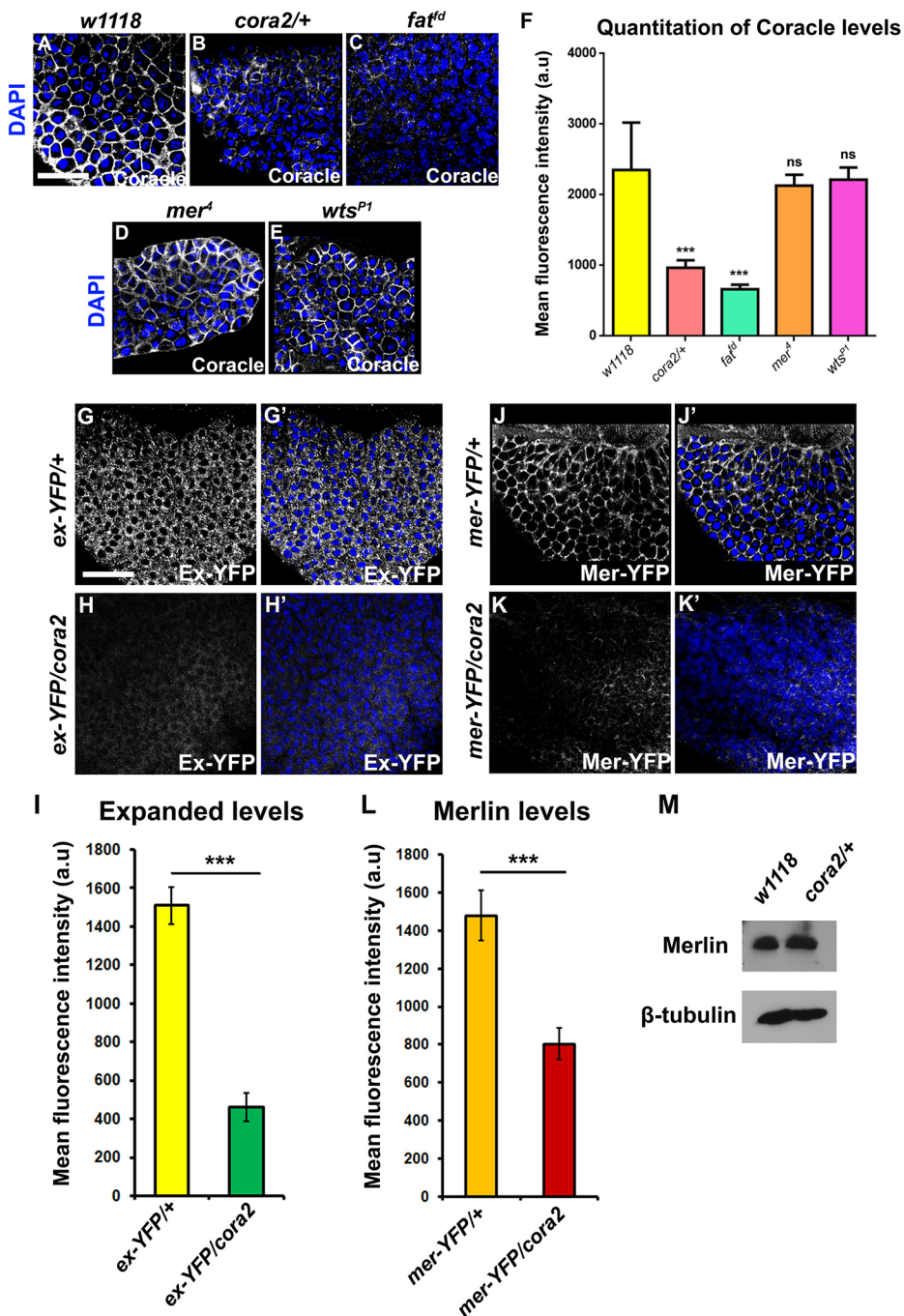
Fig. 5. Cora acts upstream of Ex and Mer.
(A-E) Representative high-magnification confocal sections of the hemocytes in the primary lymph gland lobe showing Coracle expression (white, nuclei labeled with DAPI in blue) in wild-type control (*w1118*; A), heterozygous *cora* allele (*cora2/+*; B) or homozygous mutant alleles of *fat* (*fat^fd^*; C), *merlin* (*mer^4^*; D) or *warts* (*wts^P1^*; E). (F) Quantification of Cora expression (in arbitrary units, see supplementary Materials and Methods) for genotypes shown in A-E. (G-K′) Representative high-magnification confocal sections of the hemocytes in the primary lymph glands showing Expanded or Merlin expression (using Expanded-YFP or Merlin-YFP in white, nuclei labeled with DAPI in blue) in control (G,G′,J,J′) or heterozygous *cora* mutant (H,H′,K,K′). (I,L) Quantification of Expanded and Merlin expression (in arbitrary units, see supplementary Materials and Methods) for genotypes shown in G,H and J,K, respectively. (M) Analysis of protein levels using western blotting showing levels of Merlin in lymph glands from *w1118* and *cora2/+* heterozygous mutant larvae. Statistical significance was estimated using unpaired *t*-test with Welch's correction. Error bars indicate s.e.m. for F and s.d. of the mean for I and L. ***P<0.001; ns, non-significant. Scale bars: 20 µm in A-E; 40 µm in G-K′. See also Figs S7, S9 and S11.

Crystal cell differentiation following Cora knockdown occurs via Hippo-mediated Notch activation

Our data and previous findings (Milton et al., 2014; Ferguson and Martinez-Agosto, 2014a,b) argue that the Hippo pathway regulates crystal cell differentiation. A possible way to mechanistically link the Hippo pathway and crystal cell differentiation is through Notch signaling. It has been established that in the LG the Notch pathway regulates crystal cell differentiation and Notch pathway genes such as *serrate* are a downstream target of Yorkie (Ferguson and Martinez-Agosto, 2014a,b). In particular, Notch cooperates with Lozenge to lock the hemocytes into a crystal cell differentiation program (Terriente-Felix et al., 2013). We hypothesized that, in line with the previous data, the increased production of crystal cells following depletion

of Cora in differentiating and mature hemocytes is the result of Notch pathway activation following Hippo pathway inactivation. To test this hypothesis, the activity of a Notch reporter [*E(spl)mβ-lacZ*] was assayed in larva heterozygous for alleles of *fat*, *wts*, *yorkie* or *cora* (Lai et al., 2000; Fig. S8A-E). These experiments revealed increased LacZ expression, consistent with higher Notch signaling, in *cora* mutants or upon a reduction in Hippo pathway activity. Importantly, downregulation of Notch signaling via targeted expression of the dominant-negative Notch transgene (Notch-DN) in the crystal cell lineage (using *lz*-GAL4) ameliorated the phenotype of RNAi-mediated knockdown of Cora by reducing the amounts of Hnt-expressing crystal cells that were produced (Fig. S8F-H). In contrast, overexpression of Cora did not modify the increased crystal cell differentiation observed when
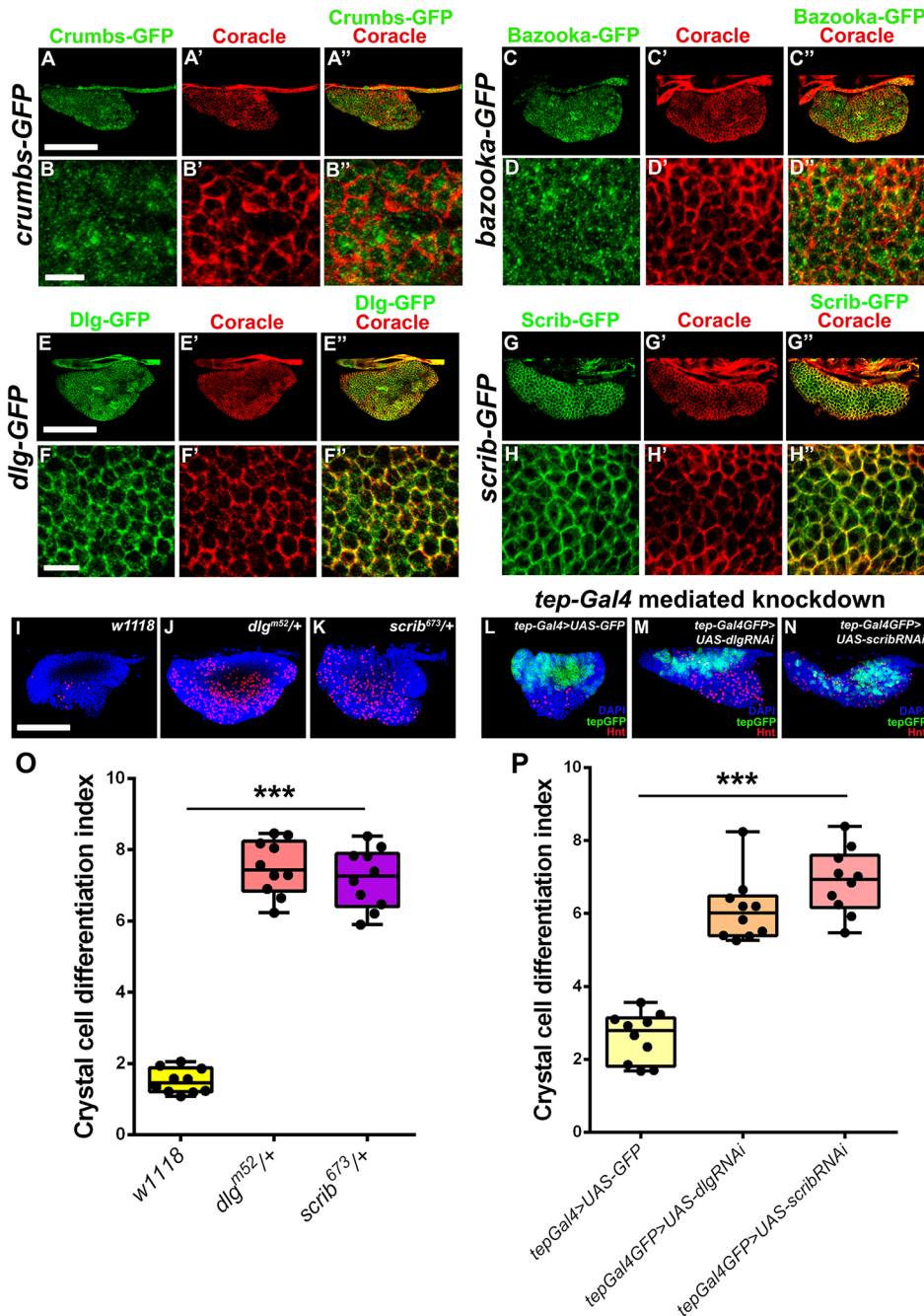
Fig. 6. Hemocytes do not exhibit distinct apicobasal polarity. (A-H″) Representative wild-type primary lymph glands showing the localization of Crumbs-GFP (A-B″, green), Bazooka-GFP (green, C-D″), Dlg-GFP (green, E-F″) and Scribble-GFP (green, G-H″). Coracle is in red. (B-B″,D-D″,F-F″,H-H″) High-magnification images showing the corresponding localization of the polarity proteins (green) and Cora (red). (I-K) Representative primary lymph gland lobes labeled for the crystal cell marker Hindsight (Hnt; red) from wild-type control larvae (*w1118*; I) and in larvae heterozygous for mutant alleles of *dlg* (*dlg^{m52}*/+; J) and *scrib* (*scrib^{673}*/+; K). (L-N) Crystal cell differentiation in representative control (UAS-GFP; L) primary lymph glands and following knockdown of *dlg* (M) and *scrib* (N) driven by the prohemocyte-specific driver *tep4-Gal4*. Crystal cells labeled for Hnt (red), prohemocyte labeled by expression of UAS-GFP (green). (O,P) Quantification of crystal cell differentiation index (in arbitrary units) for genotypes shown in I-K and L-N. Statistical significance was estimated using an unpaired *t*-test with Welch's correction. Error bars indicate s.d. of the mean. ***P<0.001. The boxes in the box and whisker plot denote the interquartile range of the data. Horizontal lines represent the median and the points show the individual data points. Whiskers are the lines outside the box that extend to the highest and lowest data values. Plot shows data for the crystal cell differentiation indices. Scale bars: 40 µm in A-A″,C-C″,E-E″, G-G″,I-K,L-N; 20 µm in B-B″,D-D″,F-F″,H-H″.

Notch signaling is activated using the NEXT transgene (UAS-NEXT) (Vaccari et al., 2008) (Fig. S8I-K). Together, these data argue that Cora and Hippo-pathway-mediated control of crystal cell differentiation involves Notch signaling.

The cellular immune response following infection occurs through Cora-mediated control of immune cells production via the Hippo pathway

Does Cora-mediated control of immune cell production via the Hippo pathway play an important functional role in fly immunity? Our previous data showed that, in the PSC, Cora levels were reduced following infection (Khadilkar et al., 2017b). Intriguingly, a similarly significant reduction in Cora expression was seen in the rest of the LG following bacterial infection with *E. coli* (Fig. 7A-E). In line with previous observations, bacterial

infection induced a robust cellular immune response observed as an increase in the production of crystal cells (Khadilkar et al., 2017a,b; Fig. 7F,G,R). A similar increase in the production of crystal cells was observed following RNAi-mediated knockdown of Cora or the Hippo pathway component Wts using the differentiating- and mature-hemocyte driver *Pxn-Gal4* (Fig. 7J, K,N,O,R). In comparison, *Pxn-Gal4*-driven RNAi-mediated knockdown of Yorkie, or overexpression of either Wts or Cora, completely blocked the ability of the larva to produce crystal cells in response to bacterial infection (Fig. 7H,I,L,M,P-R). These data argue that bacterial infection causes induction of the cellular immune response via a reduction in Cora levels in hemocytes, which in turn leads to inactivation of the Hippo pathway and the production of crystal cells. Taken together, these findings argue that Cora-mediated control of immune cell production via the
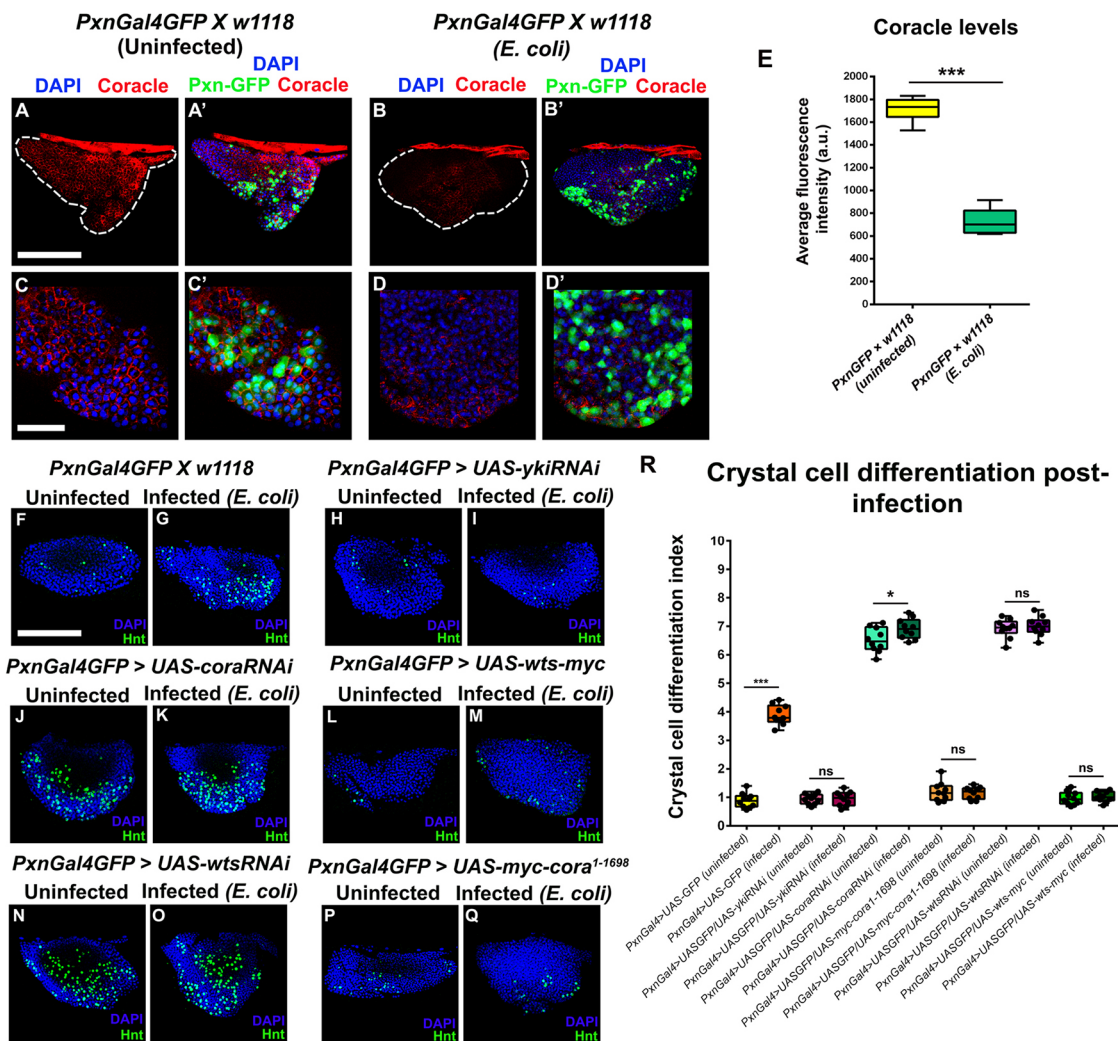
Fig. 7. Induction of crystal cell differentiation requires inactivation of Hippo signaling pathway upon bacterial infection. (A-D′) Representative confocal images of the primary lymph glands (A-B′) and high-magnification sections of the intermediate or differentiating Pxn-positive hemocytes (C-D′) in primary lymph glands showing Coracle expression (Cora in red), *Pxn-Gal4* driven GFP (green) and nuclei labeled with DAPI (blue) in uninfected wild-type control (A,A′,C,C′) and larvae infected with *E. coli* (B,B′,D,D′). (E) Quantification of Cora expression (in arbitrary units) for infected and uninfected lymph glands. (F,G) Crystal cell differentiation in representative primary lymph glands in control larvae (F) and larvae infected with *E. coli* (G). (H-Q) Crystal cell differentiation [using Hnt (green), nuclei labeled with DAPI (blue)] in representative primary lymph glands in control (H,J,L,N,P) and *E. coli*-infected (I,K,M,O,Q) larvae expressing (using *Pxn-Gal4*): UAS-*yki*-RNAi (H,I), UAS-*cora*-RNAi (J,K), UAS-*wts-myc* (L,M), UAS-*wts*-RNAi (N,O) and UAS-*myc-cora*[1-1698] (P,Q). (R) Quantification of crystal cell differentiation index (in arbitrary units) in primary lymph glands of genotypes shown in F-Q. Statistical significance was estimated using an unpaired *t*-test with Welch's correction. Error bars indicate s.d. of the mean. ***$P<0.001$, *$P<0.1$ and ns, non-significant. The boxes in the box and whisker plot denote the interquartile range of the data. Horizontal lines represent the median and the points show the individual data points. Whiskers are the lines outside the box that extend to the highest and lowest data values. Plots show data for the average fluorescence intensities (E) and crystal cell differentiation indices (R). Dotted white lines indicate the boundary of the primary lymph gland lobe in A,B. Scale bars: 40 μm in A-B′,F-Q; 20 μm in C-D′.

Hippo pathway is an important component of the fly cellular immune response.

DISCUSSION

Our work uncovers an intriguing role for septate-junction components in mediating and controlling Hippo signaling in the context of non-epithelial cells and provides a mechanistic framework for this role. Moreover, it shows that this mechanism can play an important role in controlling hematopoiesis in flies, and that this can have important functional consequences for cellular immunity. Specifically, we show that SJ components are localized to the membrane downstream of Ft, where they help to recruit and/or maintain Mer. Depletion of SJ components results in inactivation of the Hippo pathway downstream of Mer and Ex.

Robust genetic interactions between SJ and Hippo pathway components provide further support for the idea that SJs play a key role in mediating the Hippo pathway in the LG. Furthermore, we provide evidence that Hippo-mediated regulation of hemocyte differentiation downstream of SJs occurs in the blood progenitors and involves modulation of Notch signaling. Finally, we show that the induction of the cellular immune response following infection occurs, at least in part, due to a downregulation of SJ components in hemocytes as means of controlling the activity of the Hippo pathway.

This work provides insight into how Hippo signaling can adapt to function in diverse cellular contexts, particularly in non-epithelial cells, that lack apicobasal polarity. As hemocytes are not polarized in the same way that epithelial cells are, they lack modules that

typically recruit and maintain Hippo components in the apical cell cortex. It has been established in previous studies that the recruitment of Mer and Ex to the cell cortex via polarized cellular complexes, e.g. in the case of Ex through direct interactions with the Crumbs apical polarity complex, is essential for their ability to carry out their signaling function (Yin et al., 2013; Sun et al., 2015). But in hemocytes, the Crumbs complex and the apical polarity regulator Bazooka do not appear to be localized at the cell cortex, and lateral polarity markers such as Scrib and Dlg are found throughout the cell cortex. One can envisage that, in hemocytes, the lack of distinct apical cell polarization cues could impinge on proper Hippo signaling. However, this problem is overcome in the LG by using SJ components, which are present in the cell cortex of hemocytes, as means of anchoring Mer and Ex in the membrane.

By showing that the core SJ proteins Cora and NrxIV help mediate Hippo signaling in *Drosophila*, our work helps resolve an apparent inconsistency between the *Drosophila* and vertebrate Hippo signaling pathways. In vertebrates, tight junctions have been intimately linked to Hippo signaling but this did not appear to be the case for the *Drosophila* septate junctions. A convincing argument has been put forward that the role played by tight junctions in Hippo signaling in vertebrates is mediated by the sub-apical polarity complex in *Drosophila* (Karaman and Halder, 2017). This is likely true for polarized epithelial cells in flies but our work now shows that core SJ components can be directly involved in Hippo signaling in non-epithelial cells in *Drosophila*. This suggests that the role of occluding junctions in Hippo signaling is conserved in animals. Moreover, these data raise the possibility that occluding junctions might be particularly important in mediating Hippo signaling in non-epithelial tissues by acting as a substitute to the apical protein complexes that typically recruit the apically localized components of the Hippo pathway Mer and Ex.

We have recently demonstrated that SJs also play an essential role in the PSC, a region of the LG that behaves as a stem cell niche to regulate the blood cell progenitors. In addition to their function in the PSC, the results reported here suggest a separate role for SJ components that occurs in blood cell progenitors and/or in differentiating hemocytes. A few lines of evidence argue that SJs have different roles in the PSC and in prohemocytes. First, dye exclusion assays show that there is no SJ-mediated permeability barrier around the medullary zone as there is around the PSC (Khadilkar et al., 2017a,b). Second, different phenotypic rescues were observed in experiments where we restored Cora expression in the background of *cora* mutants in either the PSC, prohemocytes or crystal cells. The increased size of the LG observed in *cora* mutants was only rescued by restoring Cora in the prohemocytes, whereas increased PSC size was only rescued by restoring Cora in the PSC. In contrast, restoring Cora only in the crystal cells rescued their differentiation defects but not LG size or PSC numbers. Intriguingly, restoring Cora expression in either the PSC or prohemocytes is sufficient to rescue the increased crystal cell differentiation. As *cora*-null mutants are embryonic lethal, this might be because these rescue experiments were carried out in a *cora* heterozygous background, where overall Cora is reduced but not absent. We postulate that as there is extensive signaling between different compartments of the LG, then restoring full Cora function in one of the compartments could initiate signals that affect the behavior of another compartment in such a way as to compensate for the reduced Cora function in that compartment. Our data are thus consistent with SJs performing two spatially and temporally distinct functions in the lymph gland, by producing a permeability barrier around the PSC and by mediating Hippo signaling in hemocytes in the medullary zone.

Our genetic interaction and rescue data, as well as our localization studies, are consistent with SJ components acting upstream of Mer and Ex in the Hippo pathway in the LG, although they do not completely rule out the possibility of Cora acting in parallel. The placement of SJ components in the signaling cascade in relation to Ft is less clear. Our placement of SJ components downstream of Ft is due to the observation that they are reduced at the plasma membrane in hemocytes in the absence of Ft. However, overexpression of Ft can rescue loss of Cora, perhaps by signaling through alternative, Cora independent, mechanisms. Intriguingly, previous reports (Feng and Irvine, 2007) have suggested that Ft can regulate Wts directly, independently of Ex. A possible mechanism proposed to explain these data, the 'dual pathway hypothesis', suggest that Ft can function either through Ex or independently of Ex to ensure a robust response to signaling through Ft. This is in line with our data showing that the LG is very sensitive to the levels of Hippo signaling, given the strong phenotypes we see in heterozygous Hippo pathway mutants. In particular, if Ex-dependent and -independent pathways are acting in the LG, blocking only one, given how sensitive hematopoiesis is to the levels of Hippo signaling, is sufficient to produce a phenotype. We do not have a conclusive answer as to how Ft controls the cortical recruitment of Cora and how Cora mediates the cortical recruitment of Mer and Ex. One simple hypothesis is that tissue disorganization or other defects to the tissue caused by loss of SJs induce the mis-localization of Hippo components and inactivation of Hippo signaling. However, our data argue against this conclusion: first, we do not see tissue disorganization when we deplete SJ components either from the entire LG or specifically in the crystal cell lineage. Second, we show that activating Hippo signaling in multiple ways can fully rescue the phenotypes we observe in the LG. If SJ components were generally involved in maintaining tissue integrity in the LG, we would expect to observe some defects even if Hippo signaling function was restored.

Previous findings may provide clues into how SJ components can be involved in recruiting Mer and Ex to the membrane, especially through the SJ-associated protein Dlg. In *dlg* mutants, Hippo signaling is inactivated and there is a large increase in Yorkie activity (Sun and Irvine, 2011; Yang et al., 2015). Moreover, in the follicle cells of *Drosophila* ovaries, it has been proposed that Dlg acts together in a complex with the cell polarity regulators Scrib and Lgl as a scaffold that recruits components that are essential for Hippo signaling (Zhao et al., 2008; Enomoto and Igaki, 2011). Our data show that, similar to knockdown of SJ components, reduced *scrib* and *dlg* function promotes crystal cell differentiation. These data suggest a possible mechanistic link between Scrib/Dlg/Lgl and Cora/NrxIV, the interdependence of which is well established in polarized epithelial cells (Bilder and Perrimon, 2000; Bilder et al., 2003; Tanentzapf and Tepass, 2003), in the LG. Based on these data, we propose that the SJ components Cora and NrxIV can play a key role in the LG by mediating crosstalk between the Hippo pathway and certain parts of cellular machineries that control apicobasal polarity. This ability of SJ to mediate this crosstalk is particularly important in non-epithelial cells, where the SJs can serve as an alternative cortical polarity cue in the absence of the extensive polarization system that exists in epithelia.

MATERIALS AND METHODS
Fly stocks
RNAi lines used for all the Gal4-mediated knockdown analysis were as follows: NrxIV (JF03142, TRiP, RRID:BDSC_28715), Cora (HM05144,

TRiP, RRID:BDSC_28933), Fat (JF03245, TRiP, RRID:BDSC_29566), Expanded (JF03120, TRiP, RRID:BDSC_28703), Merlin (HMS00459, TRiP, RRID:BDSC_34958), Hippo (JF02740, TRiP, RRID:BDSC_27661), Warts (HMS00026, TRiP, RRID:BDSC_34064), Yorkie (HMS00041, TRiP, RRID:BDSC_34067), Scrib (HMS01490, RRID:BDSC_35748) and Dlg (JF01365, RRID:BDSC_25780). All other fly strains used for all the experimental analysis were either obtained from Bloomington Stock Center or were a kind gift from various fly researchers. The list is as follows: *ykiB5/ CyO* (RRID:BDSC_36290), *cora2/CyO* (RRID:BDSC_58805), *Nrx4304/ TM6B* (RRID:BDSC_4380), *fatfd/CyO, ftex13/SM6^TM6, w;sp/cyo;FRT82B wts[P1]/Tm6b, scrib[673]e[1]/TM3, Ser[1]* (RRID:BDSC_41775), *dlgm52* mutant (RRID:BDSC_36283), *hsGal4 UAS-FtHA, Four-jointed lacZ* reporter, *bantam-GFP* sensor (a gift from Dr Helen McNeill, The Lunenfeld-Tanenbaum Research Institute, Canada), *UAS-expanded* on III (a gift from Dr Georg Halder, VIB-KU Leuven, Belgium), *UAS-myc-merlin, mer4/FM7* (a gift from Dr Sarah Hughes, University of Alberta, Canada) and *ex-YFP/CyO, mer-YFP/CyO, UAS-myc-cora1-1698* (a gift from Dr Richard Fehon, University of Chicago, USA), y[1] w*; wg^Sp-1/CyO; P{UAS-dMST.FLAG}3/TM2 (RRID:BDSC_44254), w*; ft^G-rv P{neoFRT}40A/CyO; P{UAS-wts.MYC}3/TM6B, Tb[1] (RRID:BDSC_ 44258), w[*]; P{w[+mC]=UAS-wts.MYC}2/CyO; P{ry[+t7.2]=neo FRT}82B dco[3]/TM6B, Tb[1] (RRID:BDSC_44250), w*; wts^x1 P{neoFRT}82B/TM6B, Tb[1] (a gift from Dr Duojia Pan, UT Southwestern, USA), wts^MGH1/TM6B, Tb[1] (a gift from Dr Georg Halder), tep4-Gal4>UAS-GFP, lz-gal4>UAS-GFP and Pxn-Gal4>UAS-GFP (kind gifts from Dr Lucas Waltzer, GReD-CNRS/Université Clermont Auvergne, France), UAS-Notch-dominant negative(DN), UAS-NEXT (Notch constitutively active), E(spl)mbetalacZ reporter (a gift from Dr Thomas Vaccari, University of Milan, Italy), crumbs-GFP on III, dlg::GFP (CC01936), scrib::GFP (CA07683), bazooka-GFP (a gift from Dr Vanessa Auld, University of British Columbia, Canada), pebbled-Gal4 (a gift from Dr Bruce Reed, University of Waterloo, Canada), UAS-KluEnR (a gift from Dr Thomas Klein, University of Dusseldorf, Germany), eater-Gal4 (RRID: BDSC_36321), UAS-mCD8RFP on III (RRID:BDSC_32218), bantam-lacZ (RRID:BDSC_44255), UAS-mcherry scramble sponge (RRID: BDSC_61501), UAS-bantam miR sponge (a gift from Dr Vanessa Auld), thor-lacZ (RRID:BDSC_9558), w[1118]; P{ry[+t7.2]=neoFRT}43D P{w[+mC]=piM}46F P{w[+mC]=piM}47F (RRID:BDSC_2220), w[*]; P{ry[+t7.2]=neoFRT}43D cora[5]/CyO (RRID:BDSC_52233), w[*]; P{w[+mC]=UAS-FLP.Exel}3, P{w[+mC]=Ubi-p63E(FRT.STOP)Stinger} 15F2 (RRID:BDSC_28282) and Hemese-Gal4 (RRID:BDSC_8699). *w1118* was used as the wild-type control wherever required.

Drosophila genetics
Details of all the genetic crosses performed for this study are provided in the supplementary Materials and Methods.

Antibodies used
Unless otherwise indicated, all antibodies were obtained from the Developmental Studies Hybridoma Bank, Iowa, USA. Rabbit anti-GFP (1:500, A11122, Molecular Probes, A11122 RRID:AB_221569), mouse anti-Hindsight (1:50, 1G9, RRID:AB_2617420), mouse anti-Coracle [1:250, C566.9 (RRID:AB_1161642) and C615.16 (RRID: AB_1161644)], rabbit anti-Fat (1:100, a gift from Dr Helen McNeil), mouse anti-P1 (1:100, NimRodC1, a gift from Dr Istvan Ando, Biological Research Center, Hungary), rabbit anti-β-galactosidase (1:1000, Abcam ab4761, RRID:AB_449345), guinea pig anti-Expanded and -Merlin (1:1000, a gift from Dr Richard Fehon), rat anti-Pvr (1:500, a gift from Dr Denise Montell, University of California at Santa Barbera, USA) and rabbit anti Yorkie (1:1000, a gift from Dr Kenneth Irvine, Waksman Institute of Microbiology, USA). All the secondary antibodies used were obtained from Jackson Immunoresearch Laboratories. Secondary antibodies used were as follows: donkey anti-mouse Cy3 (1:400, 715-165-150), donkey anti-mouse 488 (1:400, 715-545-150), donkey anti-rabbit Cy3 (1:400, 711-165-152), donkey anti-rabbit 488 (1:400, 711-545-152), donkey anti-rat Cy3 (1:400, 712-165-153), donkey anti-guinea pig Cy3 (1:400, 706-165-148) and donkey anti-guinea pig 488 (1:400, 706-545-148).

Lymph gland dissection and immunohistochemistry
Wandering third instar larvae were used for the dissection of lymph gland. The dissections were carried out in phosphate-buffered saline (PBS), fixed in 4% paraformaldehyde (PF), followed by washes with 0.1% PTX (PBS with 0.1% Triton-X). The lymph gland preparations were then blocked with 1% normal goat serum (ab7481, Abcam) followed by overnight primary antibody incubation at 4°C. The primary antibody incubation was followed by washes with 0.1% PTX and block treatment. Appropriate Alexa-Fluor-conjugated secondary antibodies were used. The lymph gland preparations were incubated in the secondary antibody for 2 h at room temperature followed by three washes with 0.1% PTX and then mounted in VECTASHIELD with DAPI (H-1200, Vector Laboratories, RRID: AB_2336790). All the antibody dilutions were made in PBS.

Image acquisition and analysis
All images were acquired on an Olympus FV1000 inverted confocal microscope. Image analysis was performed using Olympus Fluoview (Ver.1.7c) and ImageJ software. Lymph gland boundaries have been indicated with white or brown lines. Nuclei are stained with DAPI. Analysis of mean fluorescence intensity was carried out using the ImageJ software. Analysis of mean fluorescence intensity of Cora, Expanded-YFP, Merlin-YFP and Fat levels was carried out using the ImageJ software. Mean fluorescence intensity is represented as arbitrary units. To calculate the lymph gland size, the total number of DAPI-positive nuclei in the LG (the primary lymph gland lobe and the first pair of posterior lobes were used) were estimated using the cell-counting MatLab script described by Khadilkar et al. (2017b). Images were processed using Adobe Photoshop CS3. Images were processed uniformly for brightness and contrast using Adobe Photoshop CS3 wherever needed.

Volumetric lymph gland analysis
Volumetric lymph gland analysis was carried out by counting the total number of DAPI-positive nuclei in the LG (from the primary lobe and the first pair of posterior lobes) represented in Fig. 1G. We developed custom cell-counting scripts in MatLab to measure total number of DAPI-stained cell nuclei (see supplementary Materials and Methods). This script has also been used for estimating differentiation indices in the LG and is described in a previous study (source codes 1 and 2 in Khadilkar et al., 2017b). We first filtered every image in the z-stack in the DAPI channel using a difference of Gaussians approach. A wide filter is used to remove background intensity and a smaller filter is used to remove small objects. We applied each filter to the image and subtracted the result of the smaller filter from that of the wide filter, then thresholded the final image to generate a binary mask that effectively identified cell nuclei. The script then automatically identified the bright spots within the three-dimensional image corresponding to nuclei in order to determine their numbers and centroid coordinates. This method was used to measure volumetric LG analysis shown in Fig. 1.

Larval systemic bacterial infection assay
Third instar larvae were washed three times with sterile double distilled H2O and pricked using a tungsten pin dipped in bacterial suspension of *E. coli* (OD600=200) (*E. coli* strain was a gift from Dr Bret Finlay, The University of British Columbia, Vancouver, Canada) on the postero-lateral part and then used for immunofluorescence analysis. Sucrose solution (10%) was used as a control solution for the systemic infection experiments. The infection assay was performed as described earlier (Khadilkar et al., 2017b).

Western blot analysis
Two-hundred lymph glands were dissected from *w1118* and *cora* heterozygous mutant larvae to obtain protein lysates for western blot analysis. Equal amounts of protein were loaded for both the samples. β-Tubulin was used as the housekeeping control (used at 1:100, DSHB Cat# E7, RRID: AB_528499) and the blot was probed for Merlin (using guinea pig anti-Merlin antibody, 1:10,000, a gift from Dr Richard Fehon).

Statistical analysis and significance
Each experiment was performed a minimum of three times. For all the fixed tissue analysis where the corresponding lymph glands were studied using

various antibodies, lymph glands from at least 10 individual wandering third instar larvae (n=10) were analyzed. For the post-infection (larval systemic infection assay) analysis that was carried out on lymph glands of larvae post-infection with *E. coli*, the number of lymph gland samples analyzed were from 10 larvae (n=10). Error bars represent s.d. or s.e.m., as indicated in the respective figure legends. Statistical significance was determined using an unpaired *t*-test with Welch's correction. ****P<0.0001, ***P<0.001, **P<0.01, *P<0.1 and 'ns' means non-significant. For analysis of statistical significance, each experimental sample was tested with respect to its respective control in a given experimental setup for all the data in each of the figures in order to estimate the *P*-value. Homozygous mutants were compared with the heterozygous mutant alleles as well as the wild type in order to estimate the statistical significance. Data from transheterozygotes were compared with the wild-type controls. Mutant genotypes were compared with the wild-type controls and the knockdown or overexpression genotypes were compared with their respective parental *Gal4* controls for all the statistical analysis carried out. No statistical method was used to predetermine the sample size and the experiments were not randomized.

References
Adler, P. N. (2002). Planar signaling and morphogenesis in Drosophila. *Dev. Cell* **2**, 525-535.

Anderson, A. M., Bailetti, A. A., Rodkin, E., De, A. and Bach, E. A. (2017). A genetic screen reveals an unexpected role for yorkie signaling in JAK/STAT-dependent hematopoietic malignancies in Drosophila melanogaster. *G3 (Bethesda)* **7**, 2427-2438.

Avet-Rochex, A., Boyer, K., Polesello, C., Gobert, V., Osman, D., Roch, F., Auge, B., Zanet, J., Haenlin, M. and Waltzer, L. (2010). An in vivo RNA interference screen identifies gene networks controlling Drosophila melanogaster blood cell homeostasis. *BMC Dev. Biol.* **10**, 65.

Becam, I., Rafel, N., Hong, X., Cohen, S. M. and Milán, M. (2011). Notch-mediated repression of bantam miRNA contributes to boundary formation in the Drosophila wing. *Development* **138**, 3781-3789.

Bennett, F. C. and Harvey, K. F. (2006). Fat cadherin modulates organ size in Drosophila via the Salvador/Warts/Hippo signaling pathway. *Curr. Biol.* **16**, 2101-2110.

Bilder, D. and Perrimon, N. (2000). Localization of apical epithelial determinants by the basolateral PDZ protein Scribble. *Nature* **403**, 676.

Bilder, D., Schober, M. and Perrimon, N. (2003). Integrated activity of PDZ protein complexes regulates epithelial polarity. *Nat. Cell Biol.* **5**, 53.

Brennecke, J., Hipfner, D. R., Stark, A., Russell, R. B. and Cohen, S. M. (2003). bantam encodes a developmentally regulated microRNA that controls cell proliferation and regulates the proapoptotic gene hid in Drosophila. *Cell* **113**, 25-36.

Brodsky, M. H. and Steller, H. (1996). Positional information along the dorsal–ventral axis of the drosophila eye: graded expression of the four-jointed gene. *Dev. Biol.* **173**, 428-446.

Chan, S. W., Lim, C. J., Chong, Y. F., Pobbati, A. V., Huang, C. and Hong, W. (2011). Hippo pathway-independent restriction of TAZ and YAP by angiomotin. *J. Biol. Chem.* **286**, 7018-7026.

Chen, C.-L., Schroeder, M. C., Kango-Singh, M., Tao, C. and Halder, G. (2012). Tumor suppression by cell competition through regulation of the Hippo pathway. *Proc. Natl Acad. Sci. USA* **109**, 484-489.

Cho, E., Feng, Y., Rauskolb, C., Maitra, S., Fehon, R. and Irvine, K. D. (2006). Delineation of a Fat tumor suppressor pathway. *Nat. Genet.* **38**, 1142.

Defaye, A., Evans, I., Crozatier, M., Wood, W., Lemaitre, B. and Leulier, F. (2009). Genetic ablation of Drosophila phagocytes reveals their contribution to both development and resistance to bacterial infection. *J. Innate Immun.* **1**, 322-334.

Elbediwy, A., Vincent-Mistiaen, Z. I. and Thompson, B. J. (2016). YAP and TAZ in epithelial stem cells: a sensor for cell polarity, mechanical forces and tissue damage. *BioEssays* **38**, 644-653.

Enomoto, M. and Igaki, T. (2011). Deciphering tumor-suppressor signaling in flies: genetic link between Scribble/Dlg/Lgl and the Hippo pathways. *J. Genet. Genomics* **38**, 461-470.

Evans, C. J., Hartenstein, V. and Banerjee, U. (2003). Thicker than blood: conserved mechanisms in Drosophila and vertebrate hematopoiesis. *Dev. Cell* **5**, 673-690.

Feng, Y. and Irvine, K. D. (2007). Fat and expanded act in parallel to regulate growth through warts. *Proc. Natl Acad. Sci. USA* **104**, 20362-20367.

Ferguson, G. B. and Martinez-Agosto, J. A. (2014a). Kicking it up a Notch for the best in show: Scalloped leads Yorkie into the haematopoietic arena. *Fly* **8**, 206-217.

Ferguson, G. B. and Martinez-Agosto, J. A. (2014b). Yorkie and Scalloped signaling regulates Notch-dependent lineage specification during Drosophila hematopoiesis. *Curr. Biol.* **24**, 2665-2672.

Ferguson, G. B. and Martinez-Agosto, J. A. (2017). The TEAD family transcription factor Scalloped regulates blood progenitor maintenance and proliferation in Drosophila through PDGF/VEGFR receptor (Pvr) signaling. *Dev. Biol.* **425**, 21-32.

Gao, H., Wu, X. and Fossett, N. (2013). Drosophila E-cadherin functions in hematopoietic progenitors to maintain multipotency and block differentiation. *PLoS One* **8**, e74684.

Gao, H., Wu, X., Simon, L. and Fossett, N. (2014). Antioxidants maintain E-cadherin levels to limit Drosophila prohemocyte differentiation. *PloS One* **9**, e107768.

Goodrich, L. V. and Strutt, D. (2011). Principles of planar polarity in animal development. *Development* **138**, 1877-1892.

Grusche, F. A., Degoutin, J. L., Richardson, H. E. and Harvey, K. F. (2011). The Salvador/Warts/Hippo pathway controls regenerative tissue growth in Drosophila melanogaster. *Dev. Biol.* **350**, 255-266.

Grzeschik, N. A., Parsons, L. M., Allott, M. L., Harvey, K. F. and Richardson, H. E. (2010). Lgl, aPKC, and Crumbs regulate the Salvador/Warts/Hippo pathway through two distinct mechanisms. *Curr. Biol.* **20**, 573-581.

Hoffmann, J. A., Hetru, C. and Reichhart, J.-M. (1993). The humoral antibacterial response of Drosophila. *FEBS Lett.* **325**, 63-66.

Huang, J., Wu, S., Barrera, J., Matthews, K. and Pan, D. (2005). The Hippo signaling pathway coordinately regulates cell proliferation and apoptosis by inactivating Yorkie, the Drosophila Homolog of YAP. *Cell* **122**, 421-434.

Huang, H.-L., Wang, S., Yin, M.-X., Dong, L., Wang, C., Wu, W.,Lu, Y., Feng, M., Dai, C., Guo, X. et al. (2013). Par-1 regulates tissue growth by influencing hippo phosphorylation status and hippo-salvador association. *PLoS Biol.* **11**, e1001620.

Huang, H., Li, J., Hu, L., Ge, L., Ji, H., Zhao, Y. and Zhang, L. (2014). Bantam is essential for Drosophila intestinal stem cell proliferation in response to Hippo signaling. *Dev. Biol.* **385**, 211-219.

Jung, S.-H., Evans, C. J., Uemura, C. and Banerjee, U. (2005). The Drosophila lymph gland as a developmental model of hematopoiesis. *Development* **132**, 2521-2533.

Karaman, R. and Halder, G. (2017). Cell Junctions in Hippo Signaling. *Cold Spring Harbor Perspect. Biol.* **10**, a028753.

Khadilkar, R. J., Rodrigues, D., Mote, R. D., Sinha, A. R., Kulkarni, V., Magadi, S. S. and Inamdar, M. S. (2014). ARF1–GTP regulates Asrij to provide endocytic control of Drosophila blood cell homeostasis. *Proc. Natl Acad. Sci. USA* **111**, 4898-4903.

Khadilkar, R. J., Ray, A., Chetan, D. R., Sinha, A. R., Magadi, S. S., Kulkarni, V. and Inamdar, M. S. (2017a). Differential modulation of the cellular and humoral immune responses in Drosophila is mediated by the endosomal ARF1-Asrij axis. *Sci. Rep.* **7**, 118.

Khadilkar, R. J., Vogl, W., Goodwin, K. and Tanentzapf, G. (2017b). Modulation of occluding junctions alters the hematopoietic niche to trigger immune activation. *Elife* **6**, e28081.

Krzemień, J., Dubois, L., Makki, R., Meister, M., Vincent, A. and Crozatier, M. (2007). Control of blood cell homeostasis in Drosophila larvae by the posterior signalling centre. *Nature* **446**, 325-328.

Krzemien, J., Oyallon, J., Crozatier, M. and Vincent, A. (2010). Hematopoietic progenitors and hemocyte lineages in the Drosophila lymph gland. *Dev. Biol.* **346**, 310-319.

Kulkarni, V., Khadilkar, R. J., Srivathsa, M. S. and Inamdar, M. S. (2011). Asrij maintains the stem cell niche and controls differentiation during Drosophila lymph gland hematopoiesis. *PLoS One* **6**, e27667.

Lai, E. C., Bodner, R. and Posakony, J. W. (2000). The enhancer of split complex of Drosophila includes four Notch-regulated members of the bearded gene family. *Development* **127**, 3441-3455.

Ling, C., Zheng, Y., Yin, F., Yu, J., Huang, J., Hong, Y.,Wu, S and Pan, D. (2010). The apical transmembrane protein Crumbs functions as a tumor suppressor that regulates Hippo signaling by binding to Expanded. *Proc. Natl Acad. Sci. USA* **107**, 10532-10537.

Liu, B., Zheng, Y., Yin, F., Yu, J., Silverman, N. and Pan, D. (2016). Toll receptor-mediated Hippo signaling controls innate immunity in Drosophila. *Cell* **164**, 406-419.

Lebestky, T., Chang, T., Hartenstein, V. and Banerjee, U. (2000). Specification of Drosophila hematopoietic lineage by conserved transcription factors. *Science* **288**, 146-149.

Lebestky, T., Jung, S. H. and Banerjee, U. (2003). A Serrate-expressing signaling center controls Drosophila hematopoiesis. *Genes Dev.* **17**, 348-353.

Mandal, L., Martinez-Agosto, J. A., Evans, C. J., Hartenstein, V. and Banerjee, U. (2007). A Hedgehog-and Antennapedia-dependent niche maintains Drosophila haematopoietic precursors. *Nature* **446**, 320-324.

Matakatsu, H., Blair, S. S. and Fehon, R. G. (2017). The palmitoyltransferase Approximated promotes growth via the Hippo pathway by palmitoylation of Fat. *J. Cell Biol.* **216**, 265-277.

Matis, M. and Axelrod, J. D. (2013). Regulation of PCP by the fat signaling pathway. *Genes Dev.* **27**, 2207-2220.

McCartney, B. M., Kulikauskas, R. M., LaJeunesse, D. R. and Fehon, R. G. (2000). The neurofibromatosis-2 homologue, Merlin, and the tumor suppressor expanded function together in Drosophila to regulate cell proliferation and differentiation. *Development* **127**, 1315-1324.

Meng, Z., Moroishi, T. and Guan, K.-L. (2016). Mechanisms of Hippo pathway regulation. *Genes Dev.* **30**, 1-17.

Milton, C. C., Grusche, F. A., Degoutin, J. L., Yu, E., Dai, Q., Lai, E. C. and Harvey, K. F. (2014). The Hippo pathway regulates hematopoiesis in Drosophila melanogaster. *Curr. Biol.* **24**, 2673-2680.

Minakhina, S., Tan, W. and Steward, R. (2011). JAK/STAT and the GATA factor Pannier control hemocyte maturation and differentiation in Drosophila. *Dev. Biol.* **352**, 308-316.

Nolo, R., Morrison, C. M., Tao, C., Zhang, X. and Halder, G. (2006). The bantam microRNA is a target of the hippo tumor-suppressor pathway. *Curr. Biol.* **16**, 1895-1904.

Oka, T., Remue, E., Meerschaert, K., Vanloo, B., Boucherie, C., Gfeller, D.Bader, G. D., Sidhu, S. S., Vandekerckhove, J., Gettemans, J. et al (2010). Functional complexes between YAP2 and ZO-2 are PDZ domain-dependent, and regulate YAP2 nuclear localization and signalling. *Biochem. J.* **432**, 461-478.

Pan, D. (2010). The hippo signaling pathway in development and cancer. *Dev. Cell* **19**, 491-505.

Pennetier, D., Oyallon, J., Morin-Poulard, I., Dejean, S., Vincent, A. and Crozatier, M. (2012). Size control of the Drosophila hematopoietic niche by bone morphogenetic protein signaling reveals parallels with mammals. *Proc. Natl Acad. Sci. USA* **109**, 3389-3394.

Sharma, P. and McNeill, H. (2013). Fat and Dachsous cadherins. In *Progress in Molecular Biology and Translational Science (ed. Van Roy, F.)*, Vol. 116, pp. 215-235. Academic Press.

Silva, E., Tsatskis, Y., Gardano, L., Tapon, N. and McNeill, H. (2006). The tumor-suppressor gene fat controls tissue growth upstream of expanded in the hippo signaling pathway. *Curr. Biol.* **16**, 2081-2089.

Sinenko, S. A., Mandal, L., Martinez-Agosto, J. A. and Banerjee, U. (2009). Dual role of wingless signaling in stem-like hematopoietic precursor maintenance in Drosophila. *Dev. Cell* **16**, 756-763.

Sing, A., Tsatskis, Y., Fabian, L., Hester, I., Rosenfeld, R., Serricchio, M.,Yau, N., Bietenhader, M., Shanbhag, R., Jurisicova, A. et al. (2014). The atypical cadherin fat directly regulates mitochondrial function and metabolic state. *Cell* **158**, 1293-1308.

Sinha, A., Khadilkar, R. J., Vinay, K. S., Sinha, A. R. and Inamdar, M. S. (2013). Conserved regulation of the Jak/STAT pathway by the endosomal protein asrij maintains stem cell potency. *Cell Rep.* **4**, 649-658.

Su, T., Ludwig, M. Z., Xu, J. and Fehon, R. G. (2017). Kibra and merlin activate the hippo pathway spatially distinct from and independent of expanded. *Dev. Cell* **40**, 478-490.

Sun, G. and Irvine, K. D. (2011). Regulation of Hippo signaling by Jun kinase signaling during compensatory cell proliferation and regeneration, and in neoplastic tumors. *Dev. Biol.* **350**, 139-151.

Sun, S., Reddy, B. V. V. G. and Irvine, K. D. (2015). Localization of Hippo signalling complexes and Warts activation in vivo. *Nat. Commun.* **6**, 8402.

Sweeney, L. B., Couto, A., Chou, Y.-H., Berdnik, D., Dickson, B. J., Luo, L. and Komiyama, T. (2007). Temporal target restriction of olfactory receptor neurons by Semaphorin-1a/PlexinA-mediated axon-axon interactions. *Neuron* **53**, 185-200.

Tanentzapf, G. and Tepass, U. (2003). Interactions between the crumbs, lethal giant larvae and bazooka pathways in epithelial polarization. *Nat. Cell Biol.* **5**, 46–52.

Tepass, U. (2012). The apical polarity protein network in Drosophila epithelial cells: regulation of polarity, junctions, morphogenesis, cell growth, and survival. *Annu. Rev. Cell Dev. Biol.* **28**, 655-685.

Terriente-Felix, A., Li, J., Collins, S., Mulligan, A., Reekie, I., Bernard, F., Krejci, A. and Bray, S. (2013). Notch cooperates with Lozenge/Runx to lock haemocytes into a differentiation programme. *Development* **140**, 926-937.

Thompson, B. J. and Cohen, S. M. (2006). The Hippo pathway regulates the bantam microRNA to control cell proliferation and apoptosis in Drosophila. *Cell* **126**, 767-774.

Tokusumi, T., Shoue, D. A., Tokusumi, Y., Stoller, J. R. and Schulz, R. A. (2009). New hemocyte-specific enhancer-reporter transgenes for the analysis of hematopoiesis in Drosophila. *Genesis* **47**, 771-774.

Vaccari, T., Lu, H., Kanwar, R., Fortini, M. E. and Bilder, D. (2008). Endosomal entry regulates Notch receptor activation in Drosophila melanogaster. *J. Cell Biol.* **180**, 755-762.

Verghese, S., Waghmare, I., Kwon, H., Hanes, K. and Kango-Singh, M. (2012). Scribble acts in the Drosophila fat-hippo pathway to regulate warts activity. *PloS One* **7**, e47173.

Villano, J. L. and Katz, F. N. (1995). four-jointed is required for intermediate growth in the proximal-distal axis in Drosophila. *Development* **121**, 2767-2777.

Willecke, M., Hamaratoglu, F., Kango-Singh, M., Udan, R., Chen, C. L., Tao, C., Zhang, X. and Halder, G. (2006). The fat cadherin acts through the hippo tumor-suppressor pathway to regulate tissue size. *Curr. Biol.* **16**, 2090-2100.

Woods, D. F. and Bryant, P. J. (1991). The discs-large tumor suppressor gene of Drosophila encodes a guanylate kinase homolog localized at septate junctions. *Cell* **66**, 451-464.

Yang, C.-C., Graves, H. K., Moya, I. M., Tao, C., Hamaratoglu, F., Gladden, A. B. and Halder, G. (2015). Differential regulation of the Hippo pathway by adherens junctions and apical–basal cell polarity modules. *Proc. Natl Acad. Sci. USA* **112**, 1785-1790.

Yi, C., Troutman, S., Fera, D., Stemmer-Rachamimov, A., Avila, J. L., Christian, N., Persson, N. L., Shimono, A., Speicher, D. W., Marmorstein, R. et al. (2011). A tight junction-associated Merlin-angiomotin complex mediates Merlin's regulation of mitogenic signaling and tumor suppressive functions. *Cancer Cell* **19**, 527-540.

Yin, F., Yu, J., Zheng, Y., Chen, Q., Zhang, N. and Pan, D. (2013). Spatial organization of Hippo signaling at the plasma membrane mediated by the tumor suppressor Merlin/NF2. *Cell* **154**, 1342-1355.

Yu, F.-X. and Guan, K.-L. (2013). The Hippo pathway: regulators and regulations. *Genes Dev.* **27**, 355-371.

Zeidler, M. P., Perrimon, N. and Strutt, D. I. (1999). The four-jointed gene is required in the Drosophila eye for ommatidial polarity specification. *Curr. Biol.* **9**, 1363-1372.

Zeidler, M. P., Perrimon, N. and Strutt, D. I. (2000). Multiple roles for four-jointed in planar polarity and limb patterning. *Dev. Biol.* **228**, 181-196.

Zhao, M., Szafranski, P., Hall, C. A. and Goode, S. (2008). Basolateral junctions utilize warts signaling to control epithelial-mesenchymal transition and proliferation crucial for migration and invasion of Drosophila ovarian epithelial cells. *Genetics* **178**, 1947-1971.

Zhao, B., Li, L., Lu, Q., Wang, L. H., Liu, C.-Y., Lei, Q. and Guan, K.-L. (2011). Angiomotin is a novel Hippo pathway component that inhibits YAP oncoprotein. *Genes Dev.* **25**, 51-63.
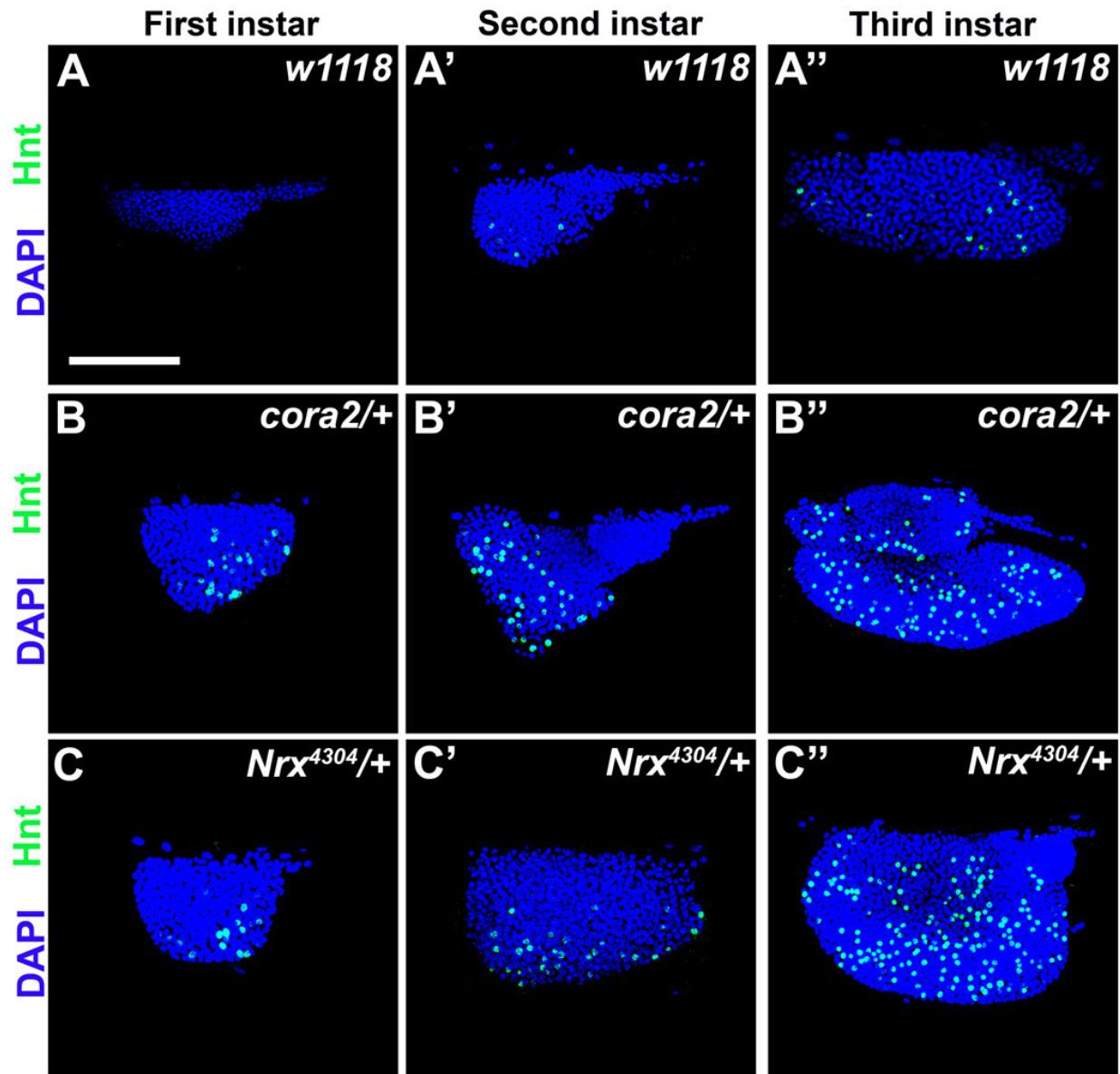
DEVELOPMENT

Supplementary figure S1

Figure S1: Septate junction component mutants show increased crystal cell differentiation from early stages of larval development. (Related to Figure 1)

(A-C) Representative primary lymph glands from first, second and third larval instar wild type control larva (*w1118*; A) and larva heterozygous for mutant null alleles of *coracle* (*cora2/+;* B) or *NrxIV* (*Nrx⁴³⁰⁴/+*; C). Crystal cells labelled with Hnt (green; Nuclei are marked with DAPI (Blue). Scale bar: 40μm (A-C'').
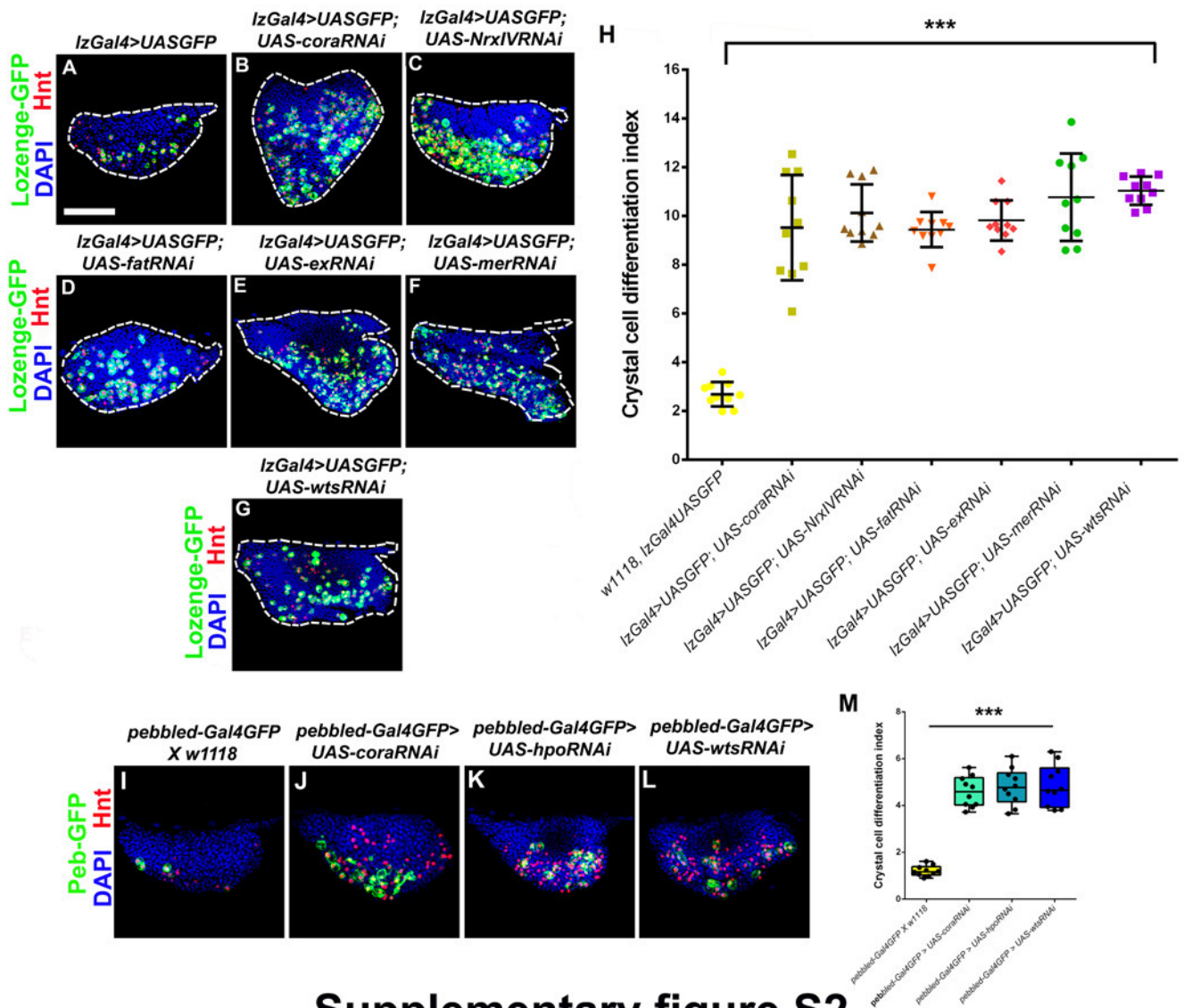
Supplementary figure S2

Figure S2: Cora and NrxIV function in the crystal cell lineage to regulate differentiation (Related to Figure 2)

(A-H) Crystal cell differentiation in representative control (UAS-GFP; A) primary lymph glands and following knockdown of *cora* (B), *NrxIV* (C), *fat* (D), *ex* (E), *mer* (F), *wts* (G) driven by the crystal cell lineage specific driver *lz-Gal4*. Crystal cells labelled with Hnt (Red), all hemocytes labelled by expression of UAS-GFP (green). (H) Quantification of crystal cell differentiation index (in arbitrary units) for genotypes shown in A-G. (I-L) Crystal cell differentiation in representative control (UAS-GFP; I) primary lymph glands and following knockdown of *cora* (J), *hippo* (K) and *warts* (L) driven by an alternate crystal cell lineage specific driver *pebbled-Gal4*. (M) Quantification of crystal cell differentiation index (in arbitrary units) for genotypes shown in I-L. Nuclei are marked with DAPI (Blue). Statistical significance was estimated using unpaired t-test with Welch's correction. Error bars indicate SD of the mean. *** indicates $P<0.001$. Scale bar: 40µm (A-G, I-L).
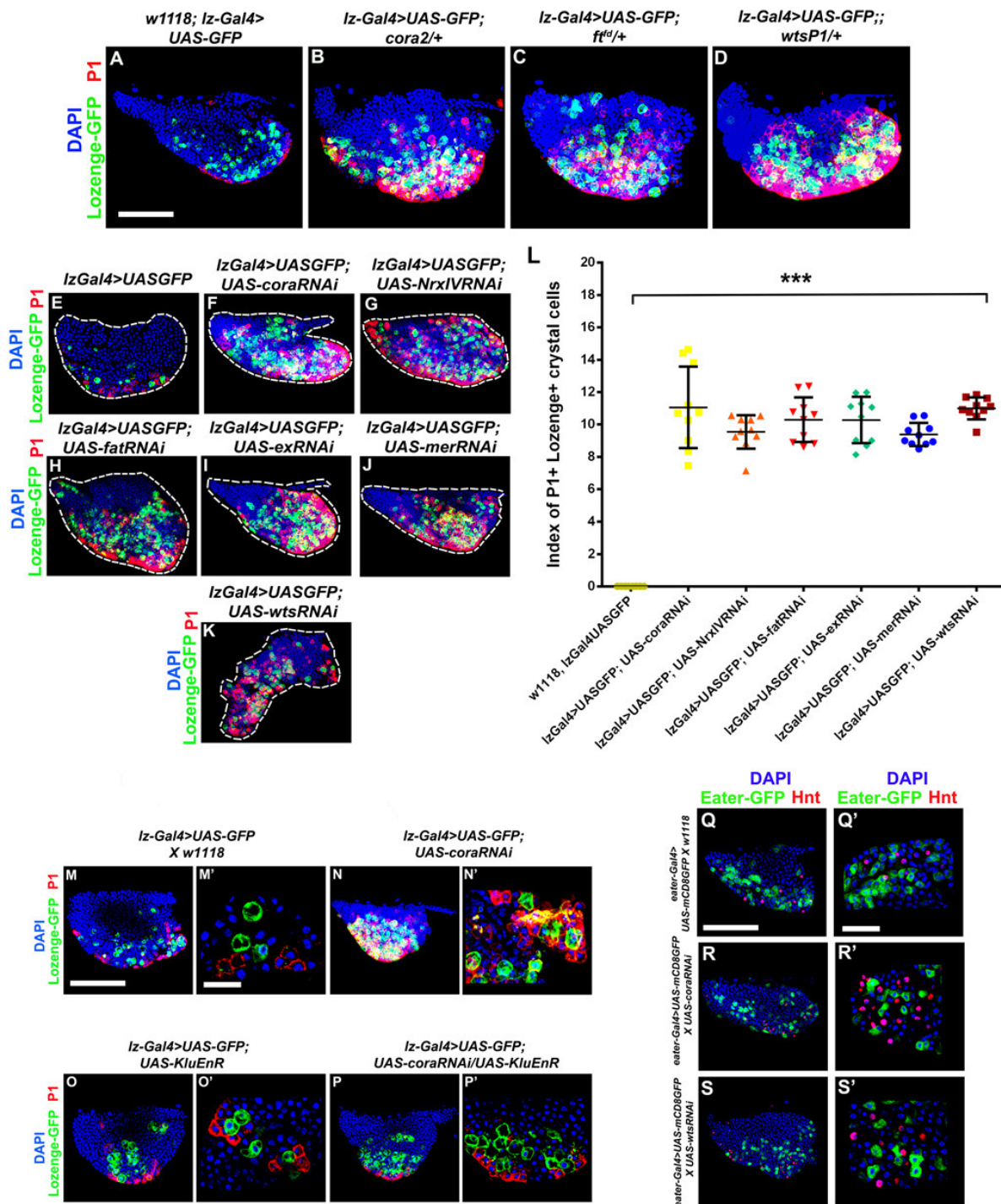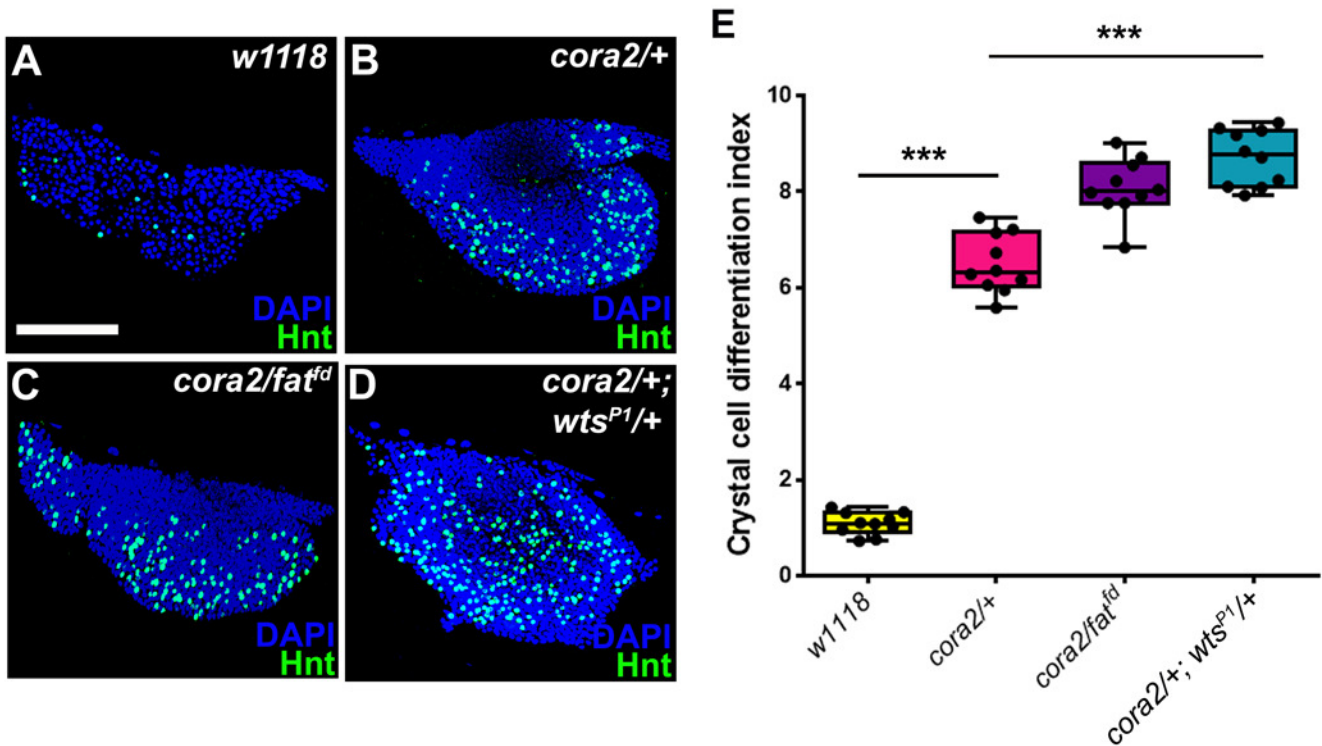
Supplementary figure S3

Figure S3: Loss of Cora, NrxIV or Hippo pathway activity results in hemocytes adopting mixed cell fate. (Related to Figure 2)

(A-D) Hemocyte differentiation in representative wild type control (*w1118*; A), heterozygous mutants for *cora* (*cora2/+*; B), *fat* (*fat^{fd}/+*; C), *wts* (*wtsP1/+*; D). Staining shown is for the crystal cell marker Lz (labelled using *lz-Gal4* to drive GFP (Green)), the plasmatocyte marker P1

(Red), and nuclei (marked with DAPI (Blue). (E-K) Hemocyte differentiation in representative primary lymph glands in control (UAS-GFP; E) or following crystal specific knockdown (using *lz-Gal4*) mediated by RNAi of *cora* (F) and *NrxIV* (G), *fat* (H), *expanded* (I), *merlin* (J), *warts* (K). Staining shown is for the crystal cell marker Lz (labelled using *lz-Gal4* to drive GFP (Green), the plasmatocyte marker P1 (Red), and nuclei (marked with DAPI (Blue). (L) Quantification of the index of dual P1/*lz-Gal4* positive (in arbitrary units, see materials and methods) for genotypes shown in E-K. (M-P) Hemocyte differentiation in representative primary lymph glands in control (*lz-Gal4>UAS-GFP X w1118*; M-M') or following crystal specific knockdown (using *lz-Gal4*) mediated by RNAi of *cora* (*lz-Gal4>UAS-GFP; UAS-coraRNAi*, N-N') or upon expression of KluEnR alone (*lz-Gal4>UAS-GFP; UAS-KluEnR,* O-O') or in the genetic background of *cora* knockdown (*lz-Gal4>UAS-GFP; UAS-coraRNAi/UAS-KluEnR,* P-P'). (M'-P') are high magnification images of hemocytes showing co-staining for crystal cells and plasmatocytes from corresponding genotypes in M-P. Staining shown is for the crystal cell marker Lz (labelled using *lz-Gal4* to drive GFP (Green), the plasmatocyte marker P1 (Red), and nuclei (marked with DAPI (Blue). (Q-S) Hemocyte differentiation in representative primary lymph glands in control (*eater-Gal4>UAS-GFP X w1118*; Q-Q') or following plasmatocyte specific knockdown (using *eater-Gal4*) mediated by RNAi of *cora* (*eater-Gal4>UAS-GFP; UAS-coraRNAi*, R-R') or *wts* (*eater-Gal4>UAS-GFP; UAS-wtsRNAi*, S-S'). (Q'-S') are high magnification images of hemocytes showing co-staining for crystal cells and plasmatocytes from corresponding genotypes in Q-S. Staining shown is for the crystal cell marker Hnt (Red), the plasmatocytes are marked by eater-Gal4 driving GFP expression (Green), and nuclei (marked with DAPI (Blue). Statistical significance was estimated using unpaired t-test with Welch's correction. Error bars indicate SD of the mean. *** indicates P<0.001. Scale bar: 40µm (A-K, M-S), 20µm (M'-S').
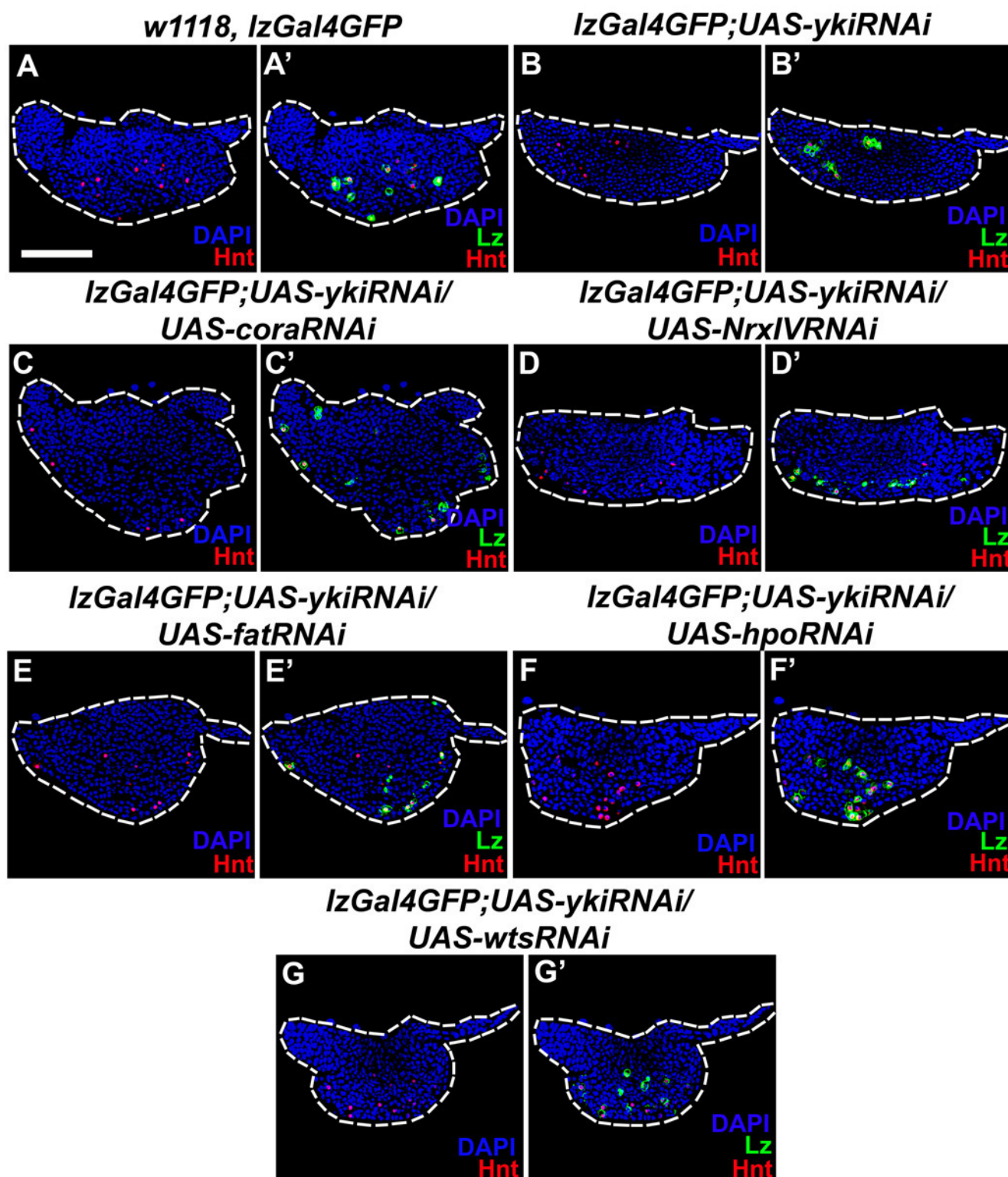
Supplementary figure S4

Figure S4: Loss of Hippo pathway components enhances the crystal cell differentiation defects caused by removing one copy of *cora* (Related to Figure 3)

(A-D) Crystal cell differentiation in representative primary lymph glands from control (*w1118*; A), heterozygous mutants for *cora* (*cora2/+*; B), double heterozygotes for *cora* and *fat* (*cora2/fatfd*; C), and *cora* and *wts* (*cora2/+*; *wtsP1/+*; D). Crystal cells labelled with Hnt (green), nuclei are marked with DAPI (Blue). (E) Quantification of crystal cell differentiation index (in arbitrary units) for genotypes shown in A-D. Statistical significance was estimated using unpaired t-test with Welch's correction. Error bars indicate SD of the mean. *** indicates P<0.001. Scale bar: 40μm (A-D).
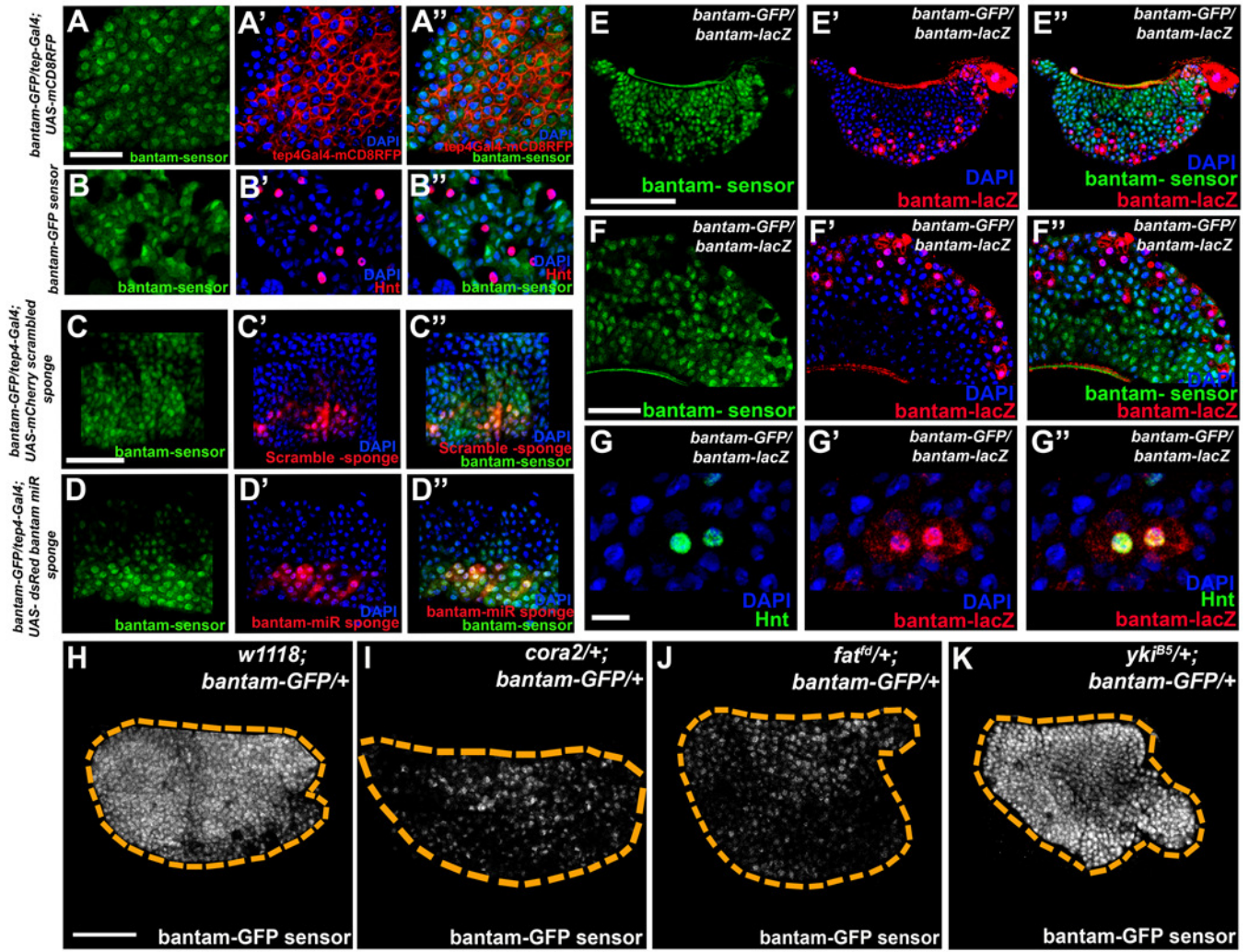
Supplementary figure S5

Figure S5: Rescue of crystal cell differentiation defects induced by knockdown of SJ or Hippo pathway components by simultaneous knockdown of *yorkie* (Related to Figure 3)

(A-G') Crystal cell differentiation in representative control primary lymph glands (w^{1118}; A-A') and following crystal cell specific (*lz-Gal4* driven) knockdown of *yorkie* by itself (B-B') or *yorkie* knockdown combined with UAS lines for the expression of RNAi lines targeting *cora* (C-C'), *NrxIV* (D-D'), *ft* (E-E'), *hippo* (F-F'), *wts* (G-G'). Crystal cells labelled with Hnt (Red), *lz-Gal4* expression marked using UAS-GFP (green), Nuclei are marked with DAPI (Blue). Scale bar: 40µm (A-G').
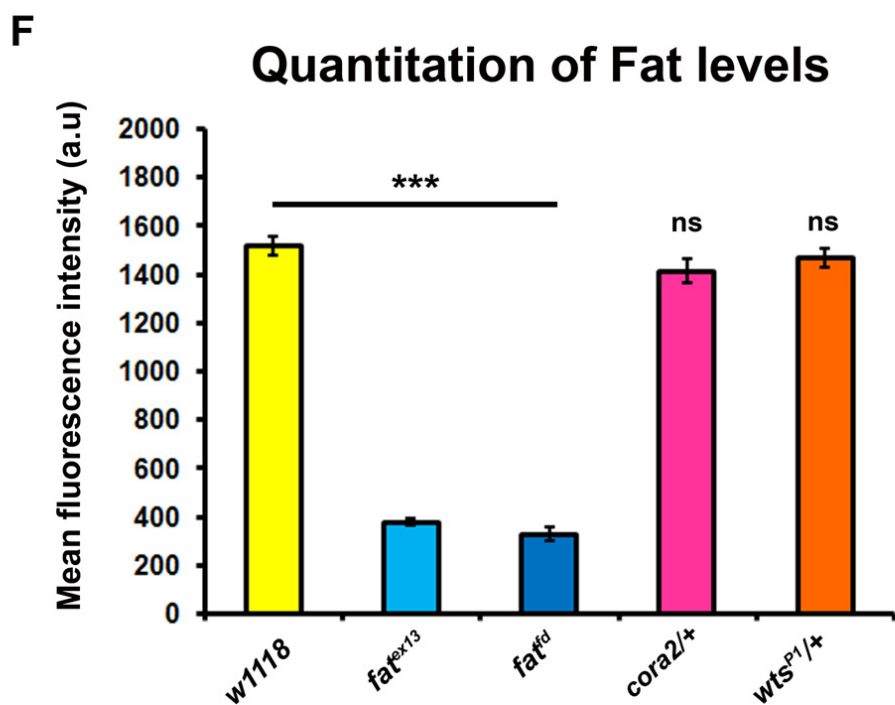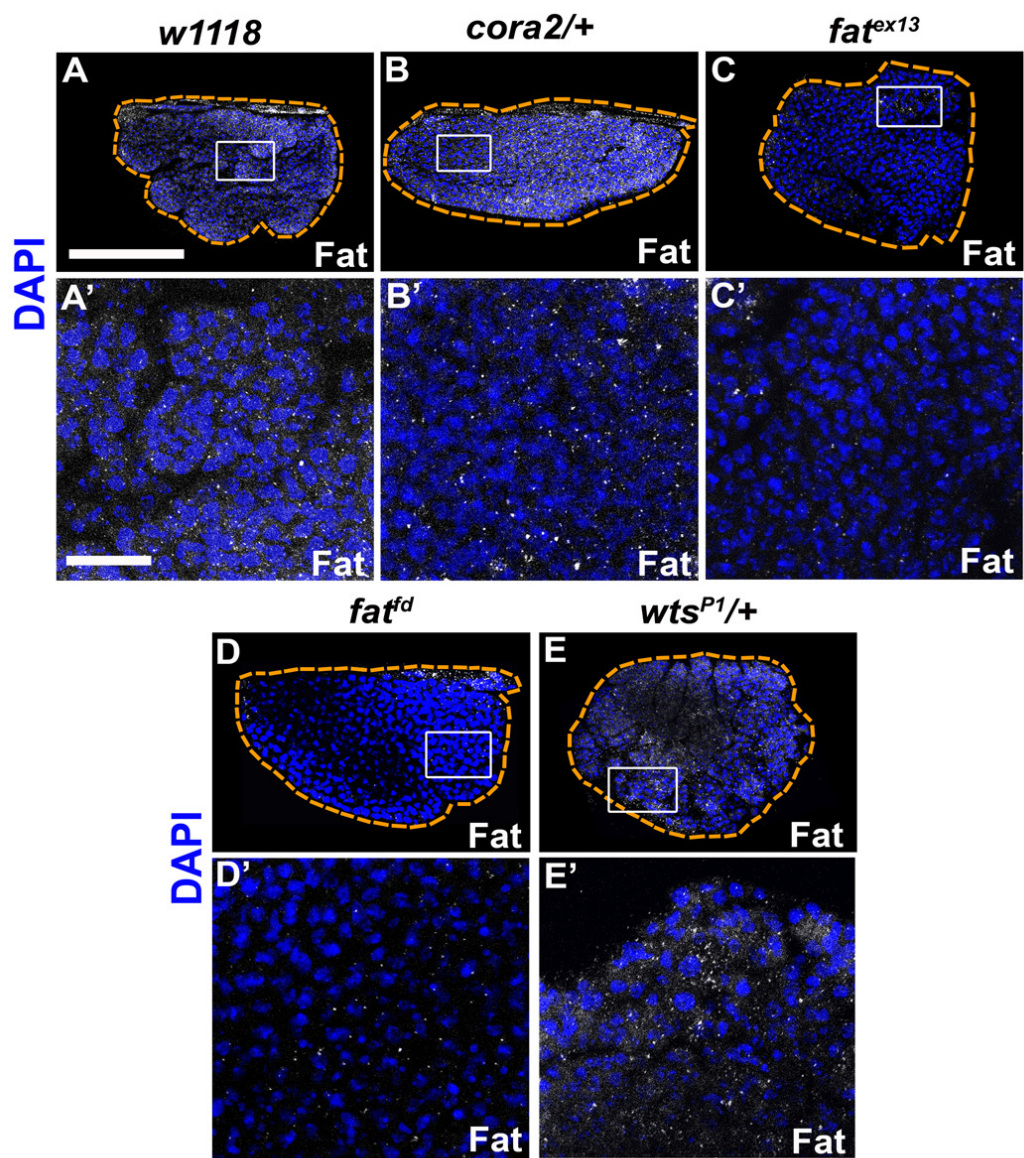
Supplementary figure S6

Figure S6: Expression of microRNA reporter *bantam-GFP* in the LG of larva with reduced levels of Cora or Hippo pathway components. (Related to Figure 3)

(A-D) Lymph gland hemocytes showing bantam-GFP sensor expression (Green) co-stained with prohemocyte marker tep-Gal4 driven UAS-mCD8RFP (Red, A-A'') or crystal cell marker Hnt (Red, B-B'') or upon *tep-Gal4* (prohemocyte specific) mediated over-expression of dsRed tagged bantam microRNA sponge (D-D'', Red) and mCherry tagged scrambled sponge (C-C'', Red). (E-F'') Lymph gland hemocytes showing bantam-GFP sensor expression (Green) and bantam-lacZ expression (Red). F-F'' are high magnification images showing bantam-GFP sensor (Green) and bantam-lacZ (Red) expression. (G-G'') Lymph gland cells marked with bantam-lacZ (Red) co-stained with crystal cell marker, Hnt (Red). (H-K) microRNA reporter, bantam-GFP sensor (white) expression in control larva (*w1118; bantam-GFP/+*; H) or larvae bearing heterozygous mutant alleles of *cora* (*cora2/+; bantam-GFP/+*; I) or components of the core Hippo pathway: *fat* (*fat^{fd}/+; bantam-GFP/+*; J) and *yorkie* (*yki^{B5}/+; bantam-GFP/+*; K). Dotted brown lines indicate the boundary of the primary lymph gland lobe. Scale bar: 40µm (E-E'', H-K), 20µm (A-D'', F-F'') and 15µm (G-G'').
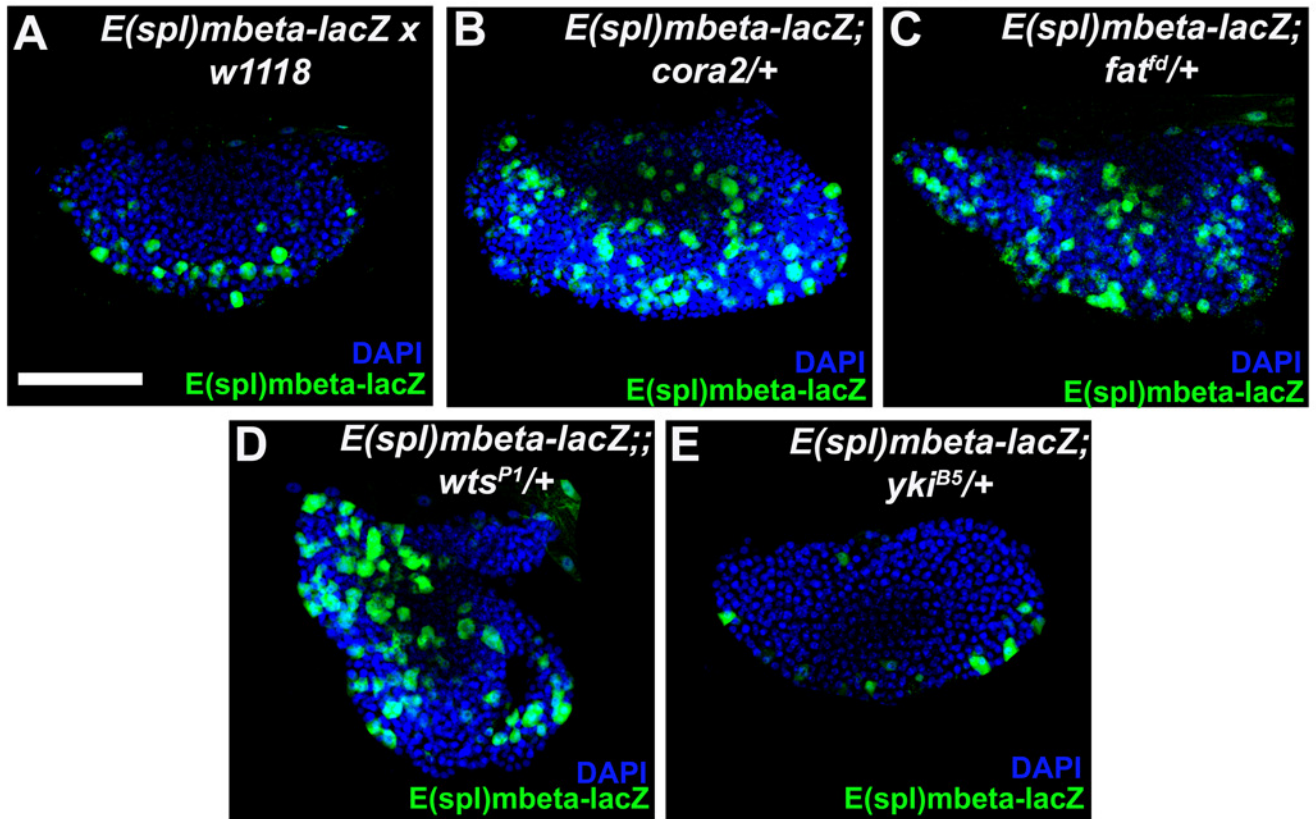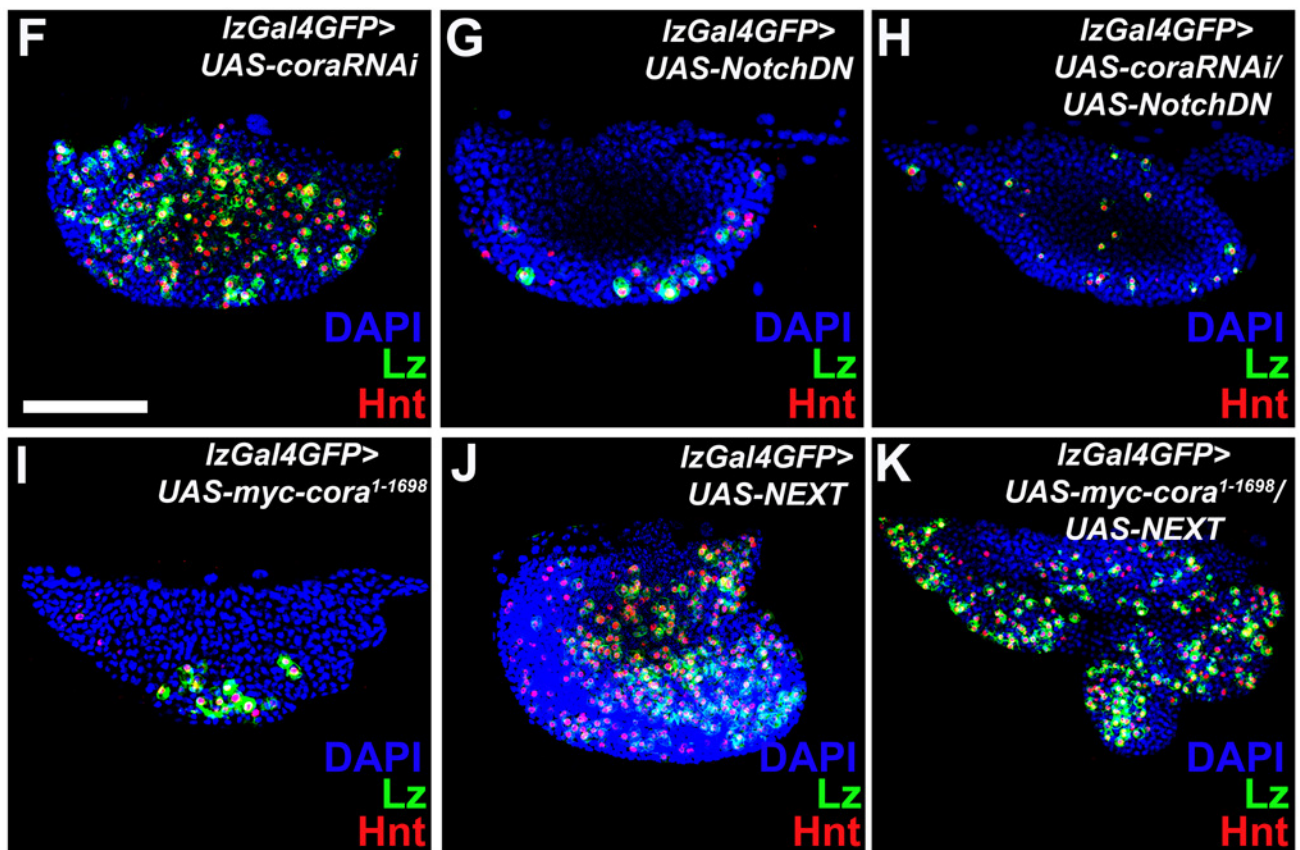
Supplementary figure S7

Figure S7: Fat localization in *cora*, *fat* and *wts* mutants. (Related to Figure 5)

(A-E) Representative high magnification confocal sections (A'-E') of the hemocytes indicated with the boxed region in the primary lymph glands showing Fat expression (white, nuclei labelled with DAPI in blue) in wild type control (*w1118*; A), heterozygous *cora* allele (*cora²/+*; B), two *fat* mutants (*fat^{ex13}*, *fat^{fd}*; C & D respectively), or heterozygous *warts* mutant (*wts^{P1}/+*; E) respectively. (F) Quantification of Fat expression (in arbitrary units, see materials and methods) for genotypes shown in A-E. For (F) Statistical significance was estimated using unpaired t-test with Welch's correction, *** indicates $P<0.001$. Error bars indicate standard error of the mean. Scale bars: 40μm (A-E), 20μm (A'-E').

Notch Reporter Activity

A *E(spl)mbeta-lacZ x w1118*
DAPI
E(spl)mbeta-lacZ

B *E(spl)mbeta-lacZ; cora2/+*
DAPI
E(spl)mbeta-lacZ

C *E(spl)mbeta-lacZ; fat^fd/+*
DAPI
E(spl)mbeta-lacZ

D *E(spl)mbeta-lacZ;; wts^P1/+*
DAPI
E(spl)mbeta-lacZ

E *E(spl)mbeta-lacZ; yki^B5/+*
DAPI
E(spl)mbeta-lacZ

Coracle-Notch pathway genetic interaction

F *lzGal4GFP> UAS-coraRNAi*
DAPI
Lz
Hnt

G *lzGal4GFP> UAS-NotchDN*
DAPI
Lz
Hnt

H *lzGal4GFP> UAS-coraRNAi/ UAS-NotchDN*
DAPI
Lz
Hnt

I *lzGal4GFP> UAS-myc-cora^1-1698*
DAPI
Lz
Hnt

J *lzGal4GFP> UAS-NEXT*
DAPI
Lz
Hnt

**K** *lzGal4GFP> UAS-myc-cora^1-1698/ UAS-NEXT*
DAPI
Lz
Hnt

Supplementary figure S8

Figure S8: Crystal cell differentiation following Cora knockdown occurs via Hippo-mediated Notch activation.

(A-E) Expression of the Notch reporter transgene *E(spl)-mbetalacZ* (in Green, nuclei labelled with DAPI in blue) in representative primary lymph glands from a wild type control (*w1118*; A*)* or larva heterozygous for mutant alleles of *cora* (*cora2/+*; B), *fat* (*fat^{fd}/+*; C), *warts* (*wts^{P1}/+*; D), and *yorkie* mutant (*yki^{B5}/*; E). (F-K) Crystal cell differentiation in representative primary lymph glands following crystal cell specific (*lz-Gal4* driven) RNAi-mediated knockdown of *cora* (F), expression of a dominant negative *notch* transgene (UAS-NotchDN) (G), or combined knockdown of *cora* and expression of dominant negative *notch* (H). (I-K) Crystal cell differentiation in representative lymph glands following crystal cell specific (*lz-Gal4* driven) over-expression of *cora* (UAS-*myc-cora*$^{1-1698}$; I), expression of a constitutively active *notch* transgene (UAS-NEXT) (J), or combined over-expression of *cora* with constitutively active *notch* (K). (F-K) Crystal cells labelled with Hnt (Red), *lz-Gal4* expression marked using UAS-GFP (green), Nuclei are marked with DAPI (Blue). Scale bar: 40µm (A-K).
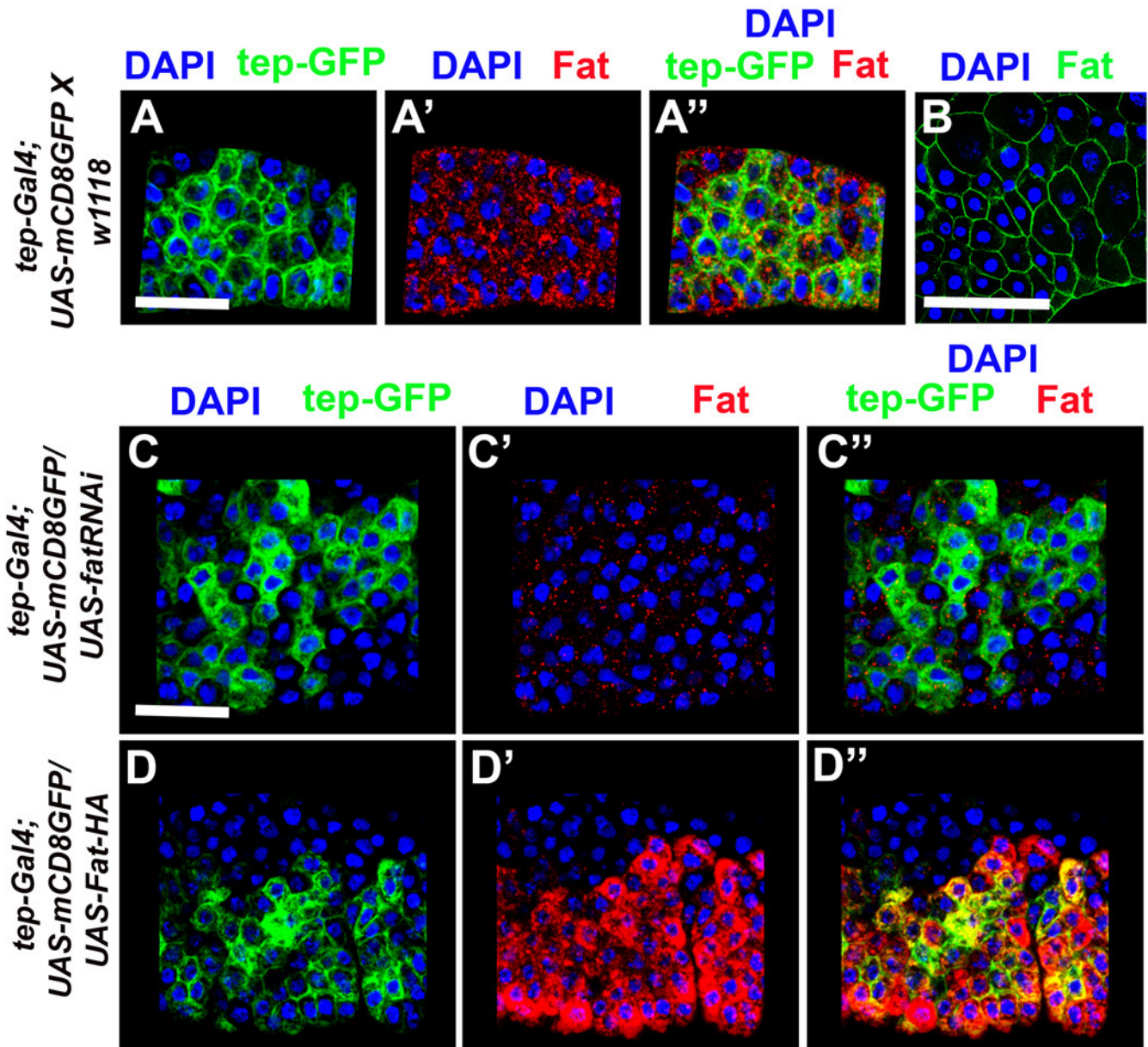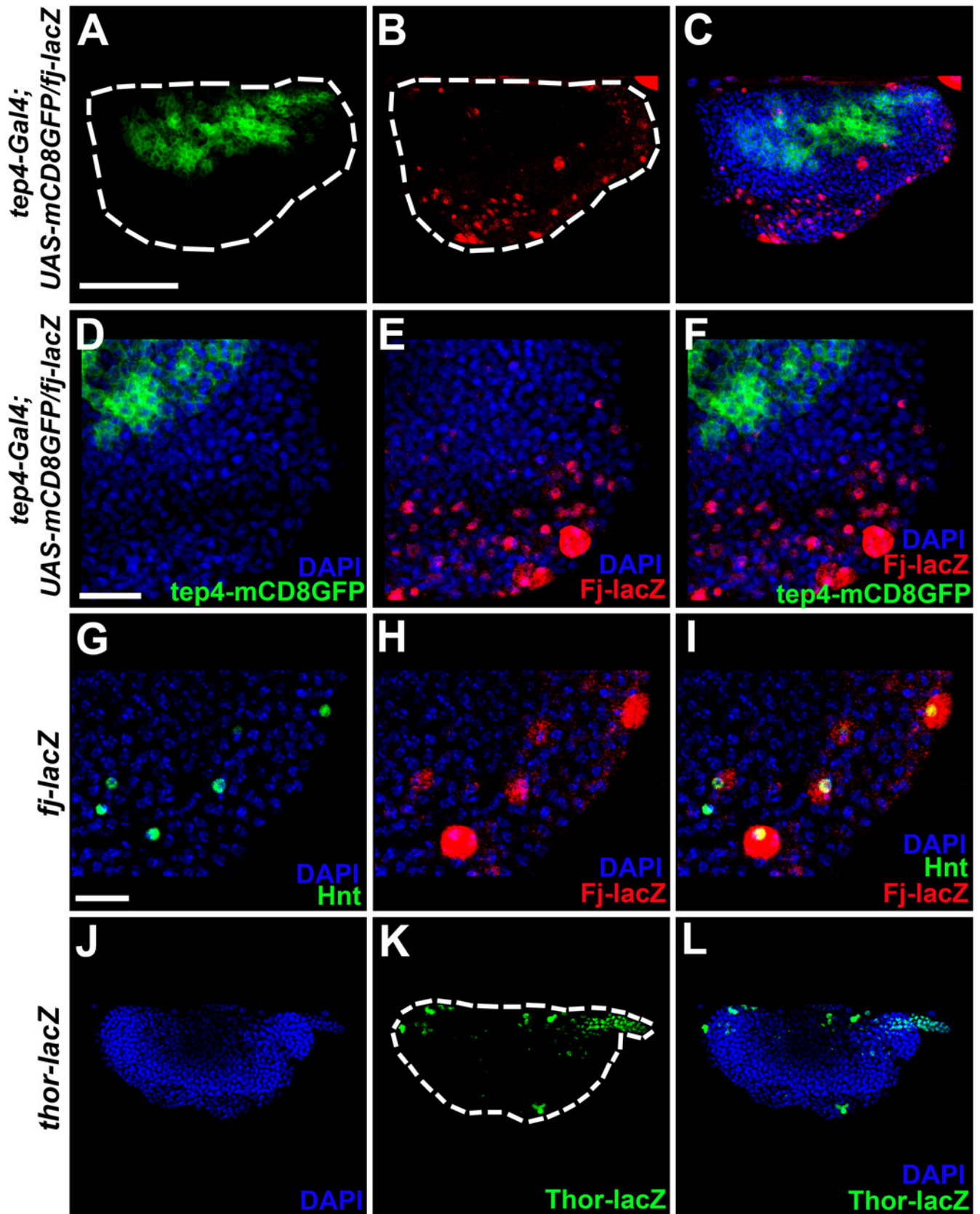
Supplementary figure S9

Figure S9: Validation of Fat expression in lymph gland hemocytes. (Related to Figure 5).

(A-A'') Expression of Fat (Red) in lymph gland prohemocytes marked with membrane tagged UAS-mCD8GFP (Green) driven by *tep4-Gal4*. (B) Fat expression (Green) in salivary gland epithelial cells. Validation of Fat expression upon knockdown (*tep4-Gal4; UAS-mCD8GFP/UAS-fatRNAi*; C-C'') or over-expression (*tep4-Gal4; UAS-mCD8GFP/UAS-Fat-HA*; D-D'') of Fat in prohemocytes using *tep4-Gal4*. Prohemocytes are marked with GFP (Green) driven by *tep4-Gal4*. Nuclei are marked with DAPI (Blue). Scale Bars: 40µm (B) 20µm (A-A'', C-D'').
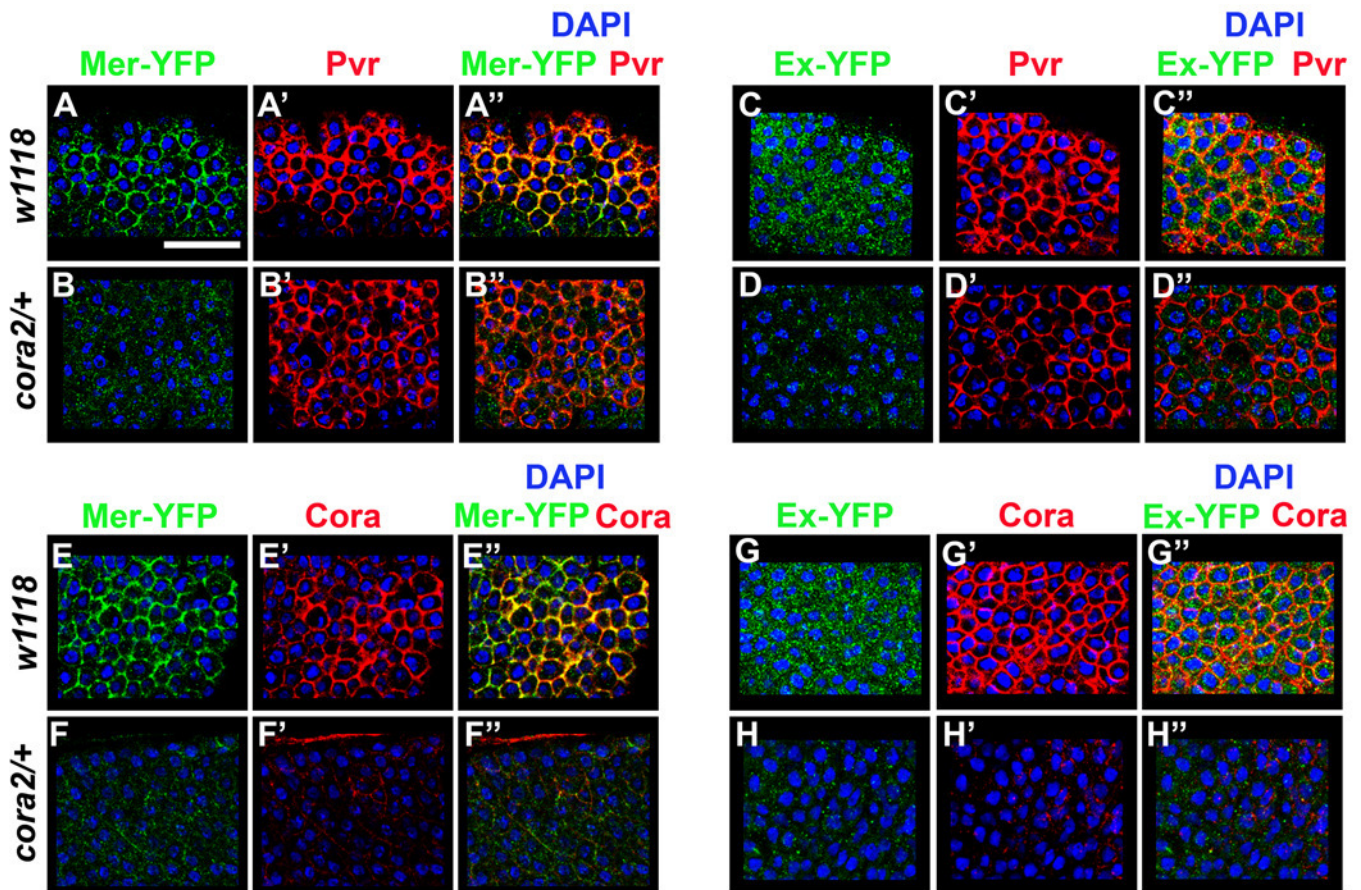
Supplementary figure S10

Figure S10: Validation of Fj-lacZ expression in lymph gland hemocytes.

(Related to Figure 3).

(A-F) Primary lymph gland lobe hemocytes showing expression of Fj-lacZ (Red) along with prohemocytes marked with GFP (Green) driven by *tep4-Gal4*. D-F are high magnification images of the corresponding primary lymph gland lobe shown in A-C. Fj-lacZ expression (Red) in lymph gland hemocytes co-stained with crystal cell marker Hnt (Green; G-I). Primary lymph gland lobe showing Thor-lacZ expression (Green) in the PSC as a lacZ control. Nuclei are marked with DAPI (Blue). Scale Bars: 40µm (A-C, J-L) 20µm (D-I).

Supplementary figure S11

Figure S11: Expanded and Merlin localization is affected in *cora* mutant lymph gland hemocytes. (Related to Figure 5).

Lymph gland hemocytes co-stained with Merlin-YFP (Green) and membrane marker Pvr (PDF-VEGF Receptor, Red) or Coracle (Red) in wild type control (*w1118*; A-A'', E-E'') and larva heterozygous for mutant null alleles of *coracle* (*cora2/+* ; B-B'', F-F''). Lymph gland hemocytes co-stained with Expanded-YFP (Green) and membrane marker Pvr (PDF-VEGF Receptor, Red) or Coracle (Red) in wild type control (*w1118*; C-C'', G-G'') and larva heterozygous for mutant null alleles of *coracle* (*cora2/+* ; D-D'', H-H''). Nuclei are marked with DAPI (Blue). Scale Bars: 20µm (A-H'').
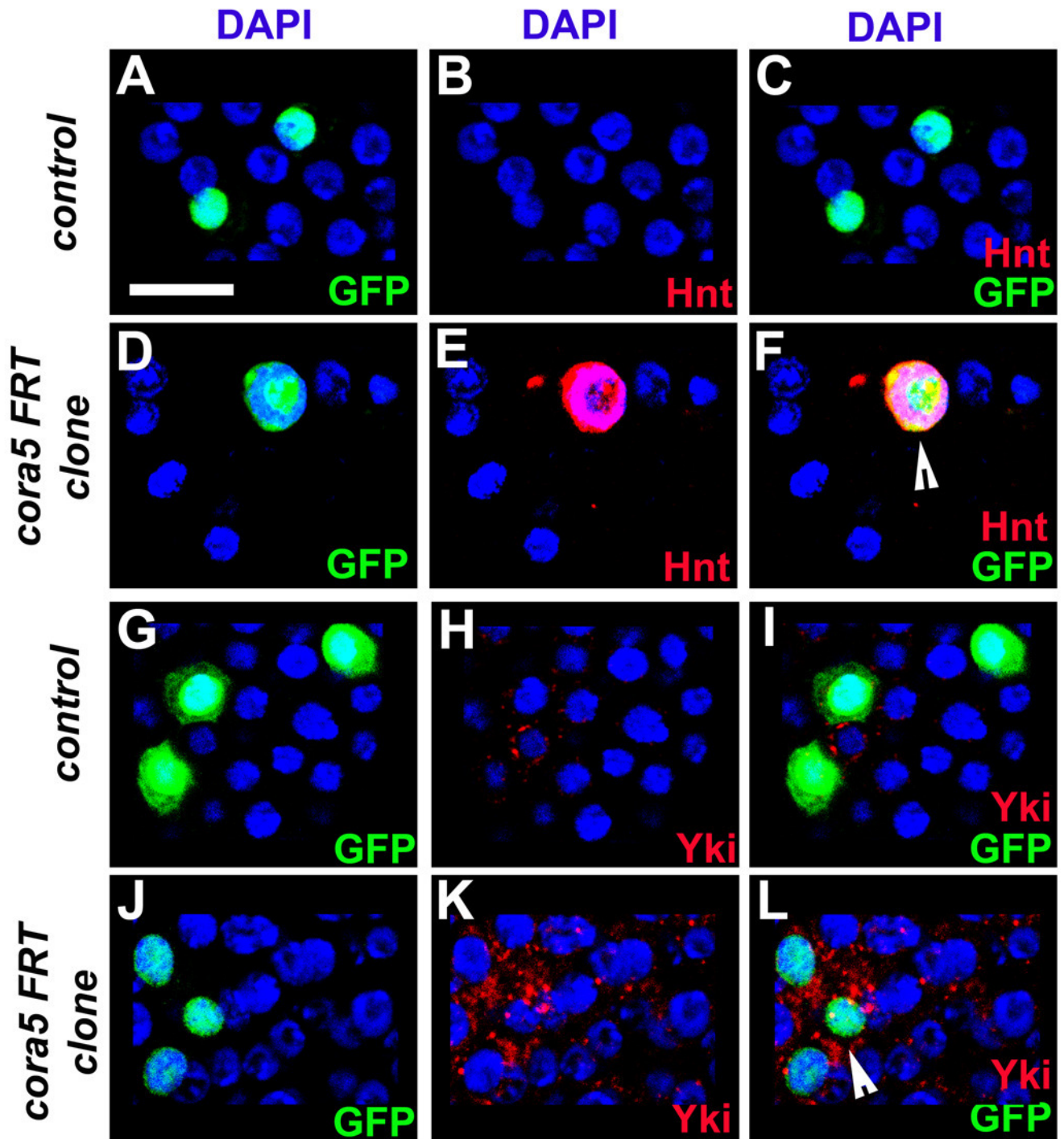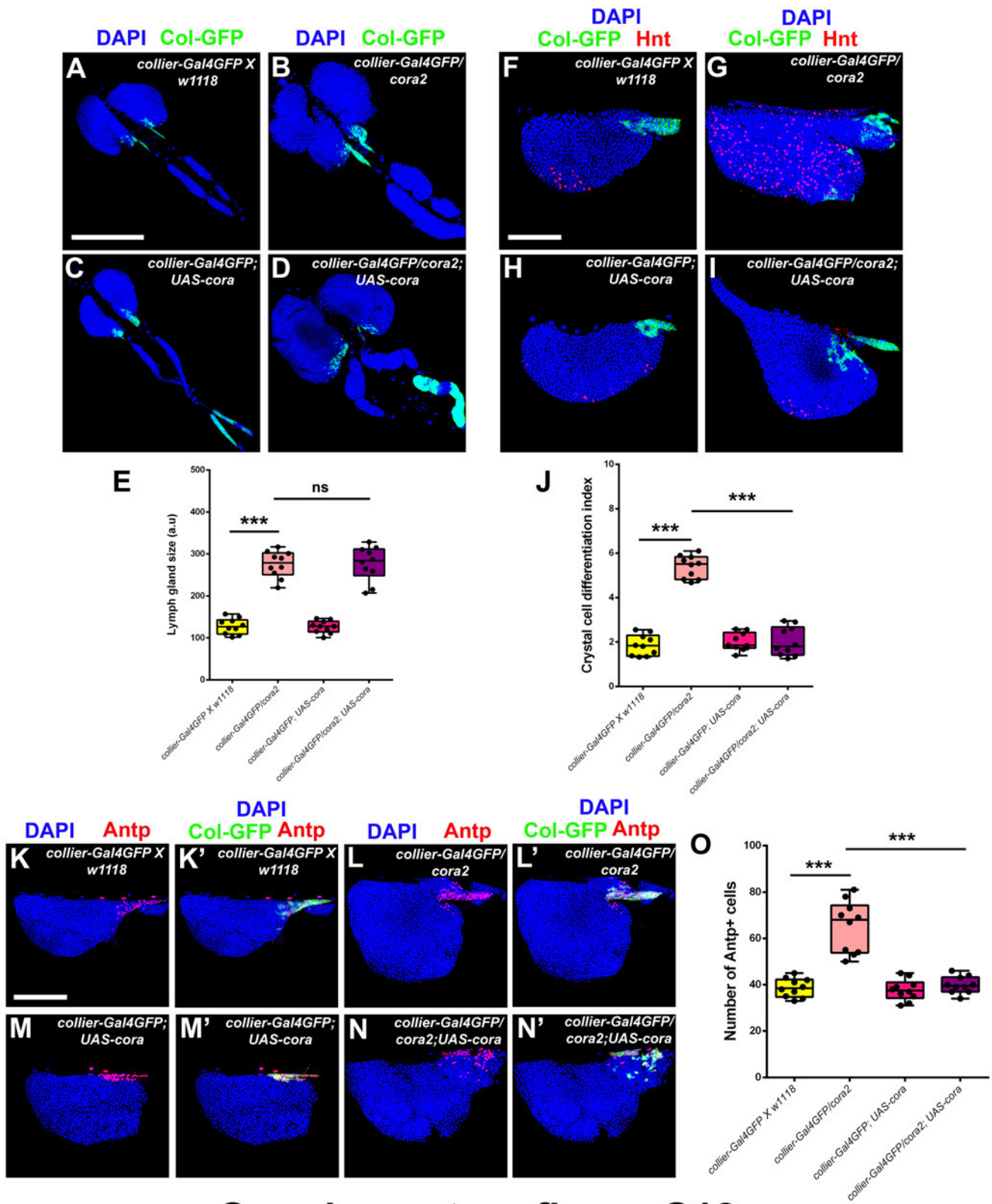
Supplementary figure S12

Figure S12: *cora* mutant clones differentiate into crystal cells and have high levels of Yorkie.

Lymph gland hemocytes consisting of GFP positive (Green) control clones (*Hemese-Gal4/ w[*];*

P{w[+mC]=UAS-FLP.Exel}3, P{w[+mC]=Ubi-p63E(FRT.STOP)Stinger}15F2; A-C, M-O) or

cora mutant clones (*FRT43D/cora5FRT43D; Hemese-Gal4/w[*]; P{w[+mC]=UAS-*

FLP.Exel}3, P{w[+mC]=Ubi-p63E(FRT.STOP)Stinger}15F2; D-F, P-R) co-stained with crystal

cell marker Hnt (Red, A-F) or Yorkie (Red, M-R). Nuclei are labelled with DAPI (Blue). Scale
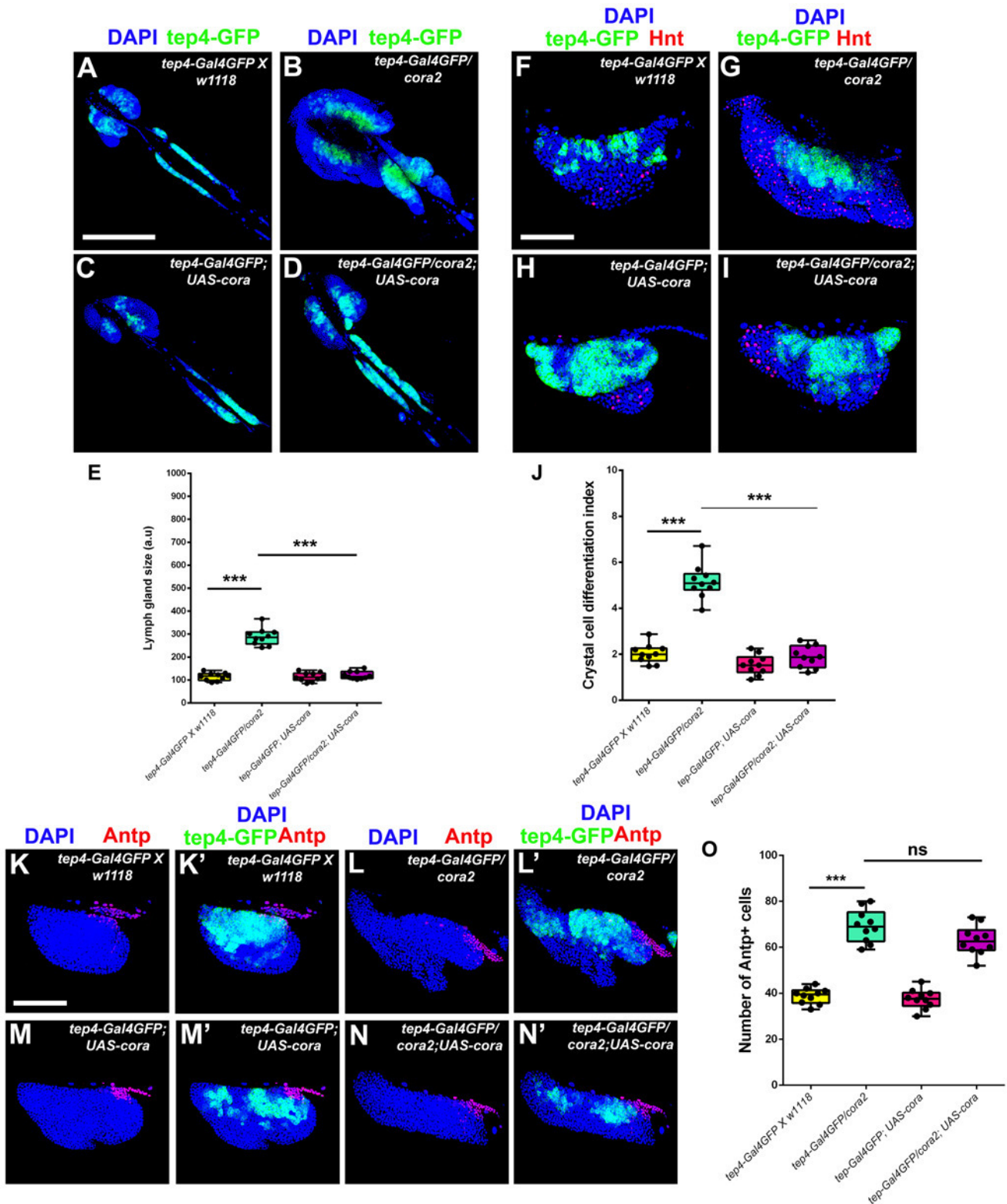
Bars: 10µm (A-R).

Supplementary figure S13

Figure S13: Coracle expression in the PSC regulates niche cell numbers and crystal cell differentiation but not the overall lymph gland size.

(A-D) Representative whole lymph glands in Gal4 control larva (*collier-Gal4GFP X w1118*; A), larva heterozygous for mutant null alleles of *coracle* (*collier-Gal4GFP/cora2;* B) or upon PSC specific over-expression of Cora alone (*collier-Gal4GFP; UAS-cora*, C) or in the *cora* mutant background (*collier-Gal4GFP/cora2; UAS-cora,* D). (E) Quantification of relative overall lymph gland organ size for genotypes shown in A-D. (F-I) Representative primary lymph gland lobes labelled with the crystal cell marker Hindsight (Hnt; Red) from Gal4 control larva (*collier-Gal4GFP X w1118*; F), larva heterozygous for mutant null alleles of *coracle* (*collier-Gal4GFP/cora2;* G), or upon PSC specific over-expression of Cora alone (*collier-Gal4GFP; UAS-cora*, H) or in the *cora* mutant background (*collier-Gal4GFP/cora2; UAS-cora,* I). (J) Quantification of crystal cell differentiation index (in arbitrary units) for genotypes shown in F-I. (K-N) Representative primary lymph gland lobes labelled with the niche cell marker Antennapedia (Antp; Red) from Gal4 control larva (*collier-Gal4GFP X w1118*; K-K'), larva heterozygous for mutant null alleles of *coracle* (*collier-Gal4GFP/cora2;* L-L'), or upon PSC specific over-expression of Cora alone (*collier-Gal4GFP; UAS-cora*, M-M') or in the *cora* mutant background (*collier-Gal4GFP/cora2; UAS-cora,* N-N'). (O) Quantification of niche cell numbers for genotypes shown in K-N'. Nuclei are marked with DAPI (Blue). PSC cells are marked with GFP (Green) driven by *collier-Gal4*. Statistical significance was estimated using unpaired t-test with Welch's correction, *** indicates $P<0.001$, ns indicates non-significant. Error bars indicate SD of the mean. Scale bars: 40µm (A-D, F-I and K-N').
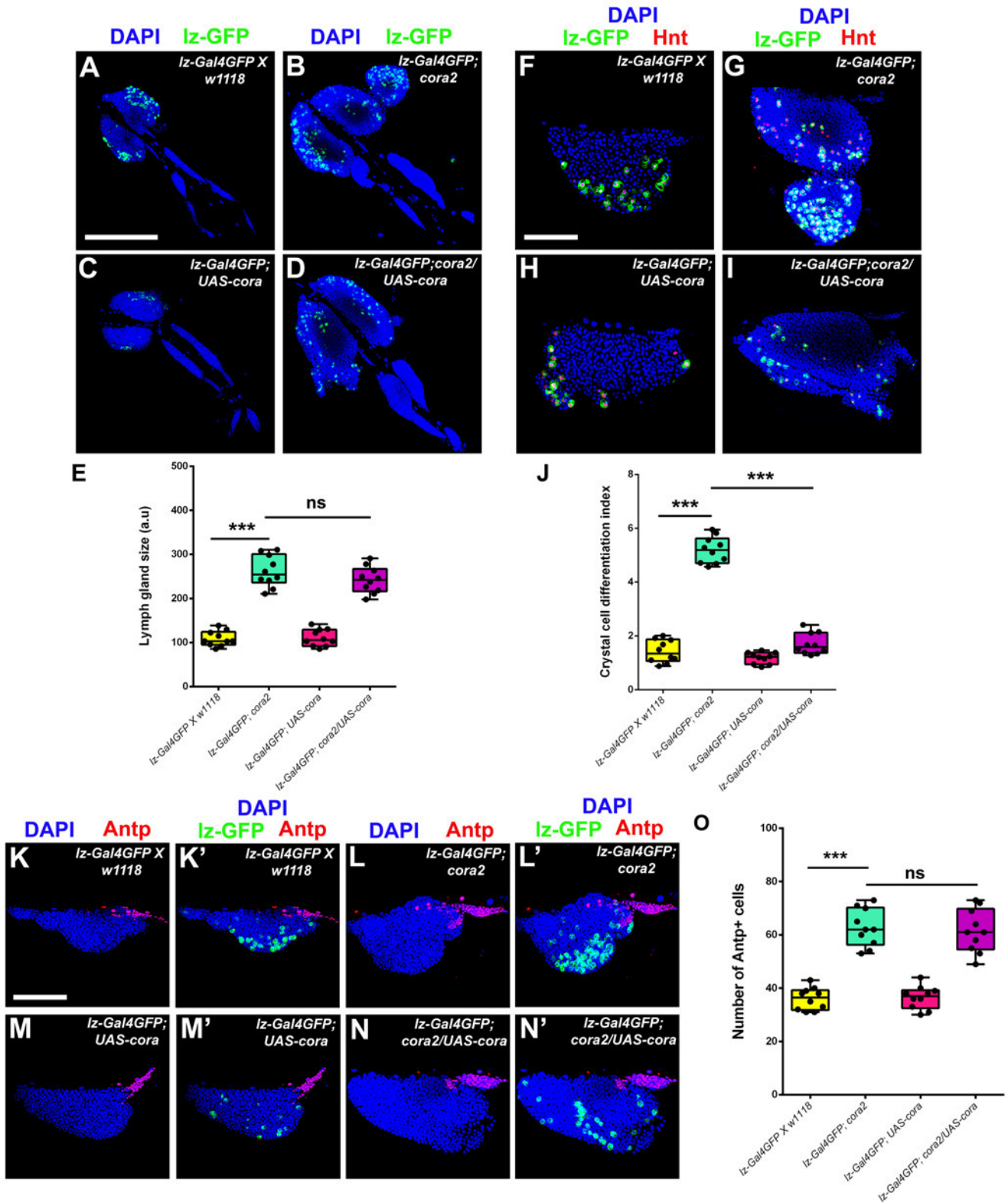
Supplementary figure S14

Figure S14: Coracle expression in the medullary zone regulates crystal cell differentiation and overall lymph gland size but not niche cell numbers.

(A-D) Representative whole lymph glands in Gal4 control larva (*tep4-Gal4GFP X w1118*; A), larva heterozygous for mutant null alleles of *coracle* (*tep4-Gal4GFP/cora2;* B) or upon medullary zone specific over-expression of Cora alone (*tep4-Gal4GFP; UAS-cora*, C) or in the *cora* mutant background (*tep4-Gal4GFP/cora2; UAS-cora,* D). (E) Quantification of relative overall lymph gland organ size for genotypes shown in A-D. (F-I) Representative primary lymph gland lobes labelled with the crystal cell marker Hindsight (Hnt; Red) from Gal4 control larva (*tep4-Gal4GFP X w1118*; F), larva heterozygous for mutant null alleles of *coracle* (*tep4-Gal4GFP/cora2;* G), or upon medullary zone specific over-expression of Cora alone (*tep4-Gal4GFP; UAS-cora*, H) or in the *cora* mutant background (*tep4-Gal4GFP/cora2; UAS-cora,* I). (J) Quantification of crystal cell differentiation index (in arbitrary units) for genotypes shown in F-I. (K-N) Representative primary lymph gland lobes labelled with the niche cell marker Antennapedia (Antp; Red) from Gal4 control larva (*tep4-Gal4GFP X w1118*; K-K'), larva heterozygous for mutant null alleles of *coracle* (*tep4-Gal4GFP/cora2;* L-L'), or upon medullary zone specific over-expression of Cora alone (*tep4-Gal4GFP; UAS-cora*, M-M') or in the *cora* mutant background (*tep4-Gal4GFP/cora2; UAS-cora,* N-N'). (O) Quantification of niche cell numbers for genotypes shown in K-N'. Nuclei are marked with DAPI (Blue). Medullary zone prohemocytes are marked with GFP (Green) driven by *tep4-Gal4*. Statistical significance was estimated using unpaired t-test with Welch's correction, *** indicates P<0.001, ns indicates non-significant. Error bars indicate SD of the mean. Scale bars: 40µm (A-D, F-I and K-N').

Supplementary figure S15

Figure S15: Coracle expression in the crystal cells cell-autonomously regulates crystal cell differentiation but does not control overall lymph gland size and niche cell numbers.

(A-D) Representative whole lymph glands in Gal4 control larva (*lz-Gal4GFP X w1118*; A), larva heterozygous for mutant null alleles of *coracle* (*lz-Gal4GFP; cora2;* B) or upon crystal cell specific over-expression of Cora alone (*lz-Gal4GFP; UAS-cora*, C) or in the *cora* mutant background (*lz-Gal4GFP; cora2/UAS-cora,* D). (E) Quantification of relative overall lymph gland organ size for genotypes shown in A-D. (F-I) Representative primary lymph gland lobes labelled with the crystal cell marker Hindsight (Hnt; Red) from Gal4 control larva (*lz-Gal4GFP X w1118*; F), larva heterozygous for mutant null alleles of *coracle* (*lz-Gal4GFP; cora2;* G), or upon crystal cell specific over-expression of Cora alone (*lz-Gal4GFP; UAS-cora*, H) or in the *cora* mutant background (*lz-Gal4GFP; cora2/UAS-cora,* I). (J) Quantification of crystal cell differentiation index (in arbitrary units) for genotypes shown in F-I. (K-N) Representative primary lymph gland lobes labelled with the niche cell marker Antennapedia (Antp; Red) from Gal4 control larva (*lz-Gal4GFP X w1118*; K-K'), larva heterozygous for mutant null alleles of *coracle* (*lz-Gal4GFP; cora2;* L-L'), or upon crystal cell specific over-expression of Cora alone (*lz-Gal4GFP; UAS-cora*, M-M') or in the *cora* mutant background (*lz-Gal4GFP; cora2/UAS-cora,* N-N'). (O) Quantification of niche cell numbers for genotypes shown in K-N'. Nuclei are marked with DAPI (Blue). Crystal cells are also marked with GFP (Green) driven by *lz-Gal4* along with Hnt (Red). Statistical significance was estimated using unpaired t-test with Welch's correction, *** indicates P<0.001, ns indicates non-significant. Error bars indicate SD of the mean. Scale bars: 40µm (A-D, F-I and K-N').

Supplemental materials and methods:

Drosophila **genetics:**

Prohemocyte specific or Intermediate/differentiating hemocyte specific RNAi or over-expression experiments were done using *tep4-Gal4* or *Pxn-Gal4* respectively. Crystal cell /maturing hemocyte specific knockdown or over-expression experiments were carried out using *lozenge-Gal4 (lz-Gal4)*. To validate the crystal cell differentiation phenotypes upon knockdown of *cora* or Hippo pathway components, an alternate crystal cell specific *pebbled-Gal4* driver was used for the crystal cell differentiation analysis. PSC specific over-expression experiments were performed using *collier-Gal4*. *eater-Gal4* was used for plasmatocyte lineage specific knockdown analysis. Heterozygous and homozygous mutants of the Hippo pathway components were used for the analysis of lymph gland tissue growth (by counting total number of cells) and crystal cell differentiation phenotypes. In addition to these, transheterozygotes of *warts* alleles were made namely: wts^{X1}/wts^{P1} and wts^{MGH1}/wts^{P1}. These alleles were originally balanced over *TM6, Tb* and upon genetic crossing; non-tubby larval progeny was selected for analysis. Total number of cells in the LG and crystal cell differentiation was analyzed in the transheterozygotes. SJ component mutant alleles or mutant alleles of the lateral polarity components Scrib or Dlg or hippo pathway mutant alleles were crossed to *w1118* (as wild type) for all the analysis using the heterozygotes. For analysis of Four-jointed expression using the Four-jointed LacZ reporter, the flies bearing the *fj-lacZ* were placed in the genetic background of either the heterozygous mutant allele of *cora* or the core hippo pathway components namely fat, *warts* and *yorkie*. To analyse whether Fj-lacZ is expressed in the lymph gland prohemocytes; *fj-lacZ* was genetically crossed to flies expressing *UAS-mCD8GFP* in the prohemocytes using *tep4-Gal4*. *thor-lacZ* was used as an unrelated lacZ control for the Fj-lacZ reporter analysis. *bantam-GFP* microRNA sensor was genetically placed in the genetic background of either the heterozygous mutant allele of *cora* or

the core hippo pathway components namely fat, *warts* and *yorkie* to analyze the transcriptional activation of Yorkie. bantam-GFP sensor was crossed to flies expressing *tep4-Gal4* driven mCD8RFP in the prohemocytes to analyze its expression in the prohemocytes. bantam-GFP sensor levels were analyzed upon expression of bantam microRNA sponge in the prohemocytes using *tep4-Gal4* as compared to the microRNA scramble sponge control. bantam-GFP sensor was also crossed to *bantam-lacZ* which reproduces the expression of the bantam microRNA to study the expression profile and validate the sensor. Double trans-heterozygotes of the mutant allele of *cora*, *NrxIV* or the core hippo pathway components with yorkie were generated to test if Yorkie genetically interacts with SJ components. To analyze Expanded and Merlin localization and recruitment in *cora* mutant genetic background, trans-heterozygotes of *expanded-YFP* or *merlin-YFP* were generated with the heterozygous mutant allele of *cora* (*cora2/CyO*). To analyze the activation of Notch pathway, Notch reporter *E(spl)mbeta-lacZ* was combined in a similar manner as *fj-lacZ* and then analyzed by staining with β-galactosidase antibody to detect β-gal positive cells. For all the *lz-Gal4, UAS-mCD8GFP* analysis; all the females used for the final genetic cross to obtain final progeny of interest had the following transgenes on their X-chromosome (*lz-Gal4, UAS-mCD8GFP/Fm7*). These females were crossed to males bearing *lz-Gal4, UAS-mCD8GFP*. These flies also contained corresponding *UAS-RNAi* or over-expression constructs on the 3rd chromosome. To study whether the crystal cells in the *cora* mutant genetic background or in the mutant background of the core hippo pathway components are dual positive for plasmatocyte antigen NimRodC1 (P1), *lz-Gal4* driving *UAS-GFP* was combined with heterozygous mutant allele of *cora* or the core hippo pathway components namely *fat* and *warts*. To study whether the dual positive differentiated hemocytes that are positive for both crystal cell and plasmatocyte markers are due to the mis-regulation of Klumpfuss; *UAS-KluEnR* (which acts as a gain of function construct upon over-expression) was over-expressed in *cora* knockdown

genetic background using crystal cell specific driver (*lz-Gal4*) to study whether the dual positive differentiated hemocyte phenotype is rescued. To check whether plasmatocyte lineage specific knockdown of *cora* or *warts* leads to the formation of dual positive differentiated hemocytes; plasmatocyte specific *eater-Gal4* was used for knockdown of *cora* or *warts* and then analyzed. Double trans-heterozygotes of the *cora* mutant allele (*cora2/CyO*) with the mutant alleles of core hippo pathway components namely *fat (fat^{fd}/CyO)* and *warts (wtsP1/Tm6Tb)* were generated to study whether they genetically act together in regulating crystal cell differentiation. To validate the Fat antibody and the expression of Fat in the lymph gland cells, Fat was depleted or over-expressed using *UAS-fatRNAi* or *UAS-fat-HA* construct. These constructs were driven in the prohemocytes using *tep-Gal4* to study Fat expression. Using FLP-FRT recombination, *cora* mutant clones were generated in the lymph gland. The construct used expresses Stinger (a nuclear-localized form of EGFP) under the control of a ubiquitin promoter upon FLP-mediated removal of an FRT cassette. *UAS-FLP* was driven by *Hemese-Gal4*. The control clones used for this analysis lacked the *cora* mutant (*cora5*) FRT allele cassette. PSC specific, MZ specific and crystal cell specific rescue analysis of the heterozygous *cora* mutant using the *UAS-cora* construct was performed using *collier-Gal4*, *tep4-Gal4* and *lz-Gal4* respectively.

Estimation of differentiation indices using MatLab:

To determine the number of differentiated crystal cells or plasmatocytes in the lymph gland, we developed custom cell counting scripts in MatLab. This script has been described and deposited in our previous study as Source code 1 and 2 (Khadilkar et al., 2017). We first filtered every image in the z-stack in the DAPI channel using a difference of Gaussians approach. A wide filter is used to remove background intensity, and a smaller filter is used to remove small objects. We applied each filter to the image and subtracted the result of the smaller filter from that of the wide filter, then thresholded the final image to generate a binary mask which effectively

identified cell nuclei. The script then automatically identified the bright spots within the 3 dimensional image corresponding to nuclei in order to determine their numbers and centroid coordinates. To calculate differentiation index, we determined what proportion of these cells also expressed markers for differentiation. The differentiation index was then calculated as follows: Differentiation index = Number of cells positive for differentiation marker identified by the script/total number of DAPI positive cells identified by the script. The index has been represented as a percentile. For each cell nucleus identified, we automatically measured intensity in the red channel within a search radius around the nucleus centroid. The search radius was defined as 1.5 times the average radius of nuclei. Nuclei surrounded by above threshold intensity in the red channel were considered differentiated. These numbers were then used to calculate the crystal cell differentiation indices or the total number of plasmatocytes. Index of dual positive crystal cells (for Lz-GFP and plasmatocyte marker, P1) was estimated by quantifying total GFP positive crystal cells overlapping with the P1 marker (Red) and then calculating the percentile of these dual positive cells with the total number of cells in the primary lymph gland lobe. In addition to this, Fj- LacZ reporter activity was analyzed by estimating the Fj-LacZ positive cells in the genetic background of heterozygous mutant allele of *cora* or core hippo pathway components was analyzed using this MatLab script and then plotted as an index of Fj-LacZ positive cells with respect to total number of cells in the primary lymph gland lobe. Number of larvae from which lymph glands were analyzed for all of the above analysis is 10 (n=10).